DOI:10.14753/SE.2023.2807

The Assessment of Diabetic Retinal Pathology using Artificial Intelligence and an Animal Model

PhD thesis

Kornélia Lenke Laurik-Feuerstein, MD

Doctoral School of Clinical Medicine
Semmelweis University

Supervisor: Gábor Márk Somfai, MD, Ph.D.
External advisor: Delia Cabrera DeBuc, Ph D., associate professor, Bascom Palmer Eye Institute, USA

Official reviewers: Szepessy Zsuzsanna, MD, Ph.D.
Hargitai János, MD, Ph.D.

Head of the Final Examination Committee: Fidy Judit, MD, D.Sc.

Members of the Final Examination Committee:
Katalin Gombos, MD, Ph.D.
Miklós Resch, MD, Ph.D.

Budapest
2023

DOI:10.14753/SE.2023.2807

TABLE OF CONTENTS

DOI:10.14753/SE.2023.2807

DOI:10.14753/SE.2023.2807

DOI:10.14753/SE.2023.2807

LIST OF ABBREVATIONS

AAO	American Academy of Ophthalmology
AI	artificial intelligence
ANN	artificial neural network
CNN	convolutional neural network
CSME	clinically significant macular edema
DL	deep learning
DM	diabetes mellitus
DME	diabetic macular edema
DNP	diabetic neuropathy
DR	diabetic retinopathy
ETDRS	Early Treatment Diabetic Retinopathy Study
FD	fractal dimension
FN	false negative
FP	false positive
GCL	ganglion cell layer
IDF	International Diabetes Federation
ILM	inner limiting membrane
INL	inner nuclear layer
IPL	inner plexiform layer
IQR	interquartile range
IS	photoreceptor inner segment
MDR	mild non-proliferative diabetic retinopathy
ML	machine learning
NPDR	non-proliferative diabetic retinopathy
OLM	outer limiting membrane
ON	optic nerve
OCT	optical coherence tomography
OCTRIMA	OCT retinal image analysis
ONL	outer nuclear layer
OPL	outer plexiform layer

OS	photoreceptor outer segment
PB	phosphate buffer
PDR	proliferative diabetic retinopathy
PPV	positive predictive value
RGC	retinal ganglion cells
RNFL	retinal nerve fiber layer
RPE	retinal pigment epithelium
SD	standard deviation
T1DM	type-1 diabetes mellitus
T2DM	type-2 diabetes mellitus
TH	thickness measurement
TN	true negative
TP	true positive
ZDF	Zucker Diabetic Fatty rat

1. INTRODUCTION

The mammalian retina is a neuroectodermal tissue specialized in detecting and transforming light into electric impulses. The retina consists of six main types of neural and additional glial cells in a highly organized arrangement, which in combination with its relatively easy histological harvesting and isolation methods makes it a widely used and popular model in neuroscience. Diabetes mellitus (DM) is a systemic disease affecting several organ systems through microangiopathy and neurodegeneration. The complications associated with DM are a severe burden on modern societies, which is also due to its socioeconomic impact.

In the present work we assess the retinal changes associated with diabetes mellitus in a clinical setting and in an animal model, coupled with some aspects in the development of automated screening tools for diabetic retinopathy (DR).

1.1. The structure of the mammalian retina

The mammalian retina can be divided into two parts based on its sensitivity to light impulses. The area separating these two parts is called the ora serrata. The light-sensitive part can be divided into the retinal pigment epithelium (RPE) and the neural retina. The latter consists of several layers of cell bodies and dendrites in the following order from the RPE towards the vitreous: outer segments (OS); inner segments (IS) and nuclei (outer nuclear layer – ONL) of the photoreceptors; outer plexiform synaptic layer (OPL); inner nuclear layer (INL) including the cell bodies of bipolar, amacrine, and horizontal cells; inner plexiform layer (IPL); and finally the cell bodies (ganglion cell layer – GCL) and axons (retinal nerve fiber layer - RNFL) of the retinal ganglion cells. The RNFL runs into and builds the optic nerve (ON), forwarding the electric impulses towards specific cerebral regions [1]. Finally, there are two further retinal layers mainly built up by the pedicles of the Müller glia cells, and the outer and inner limiting membranes (OLM and ILM) [2].

1.1.1. The histological particularities of the human and rat retinas

In contrast to other mammals, the primate retina has an approximately 5500 μm diameter area located in the visual axis, called the macula lutea. In the central 250-350 μm of the fovea is the foveola, containing exclusively a large number of cones. Moving

outwards, the density of cones decreases until it reaches rod dominance outside the macula lutea [3, 4]. Moreover, the vasculature of the human retina forms a temporal and nasal arcade, whereas the capillaries border the central foveal avascular zone.

Rats, being nocturnally active animals, have retinas with general rod dominance and only a fraction of the cone density of the human retina [5]. There is no macula lutea or fovea on the posterior pole; rats instead have a broad longitudinal zone called the visual streak with a higher proportion of cone photoreceptors. As opposed to the human retina, the retinal blood vessels are radially organized [4, 6].

1.1.2. Zucker Diabetic Fatty rat – animal model of type 2 diabetes mellitus

A number of different animal models of type 2 diabetes mellitus (T2DM) are available that develop a partial or complete insulin deficiency-induced hyperglycemia, insulin resistance, and a pancreatic β-cell deficiency mostly but not necessarily accompanied by obesity, which is a key component of T2DM. This obesity can be caused by a spontaneous or voluntary mutation of leptin or its receptor [7]. In our studies, we used Zucker Diabetic Fatty rats (ZDF) in which T2DM occurs in the males at the age of 8-10 weeks as a result of a leptin receptor mutation and a hitherto unidentified transcriptional β-cell defect [8]. The leptin receptor homozygous recessive rats (ZDFfa/fa) become obese with significantly elevated glycosylated hemoglobin, free fatty acid, triglyceride, and cholesterol; from the age of twelve weeks they have persistently elevated blood glucose levels [9, 10]. As a result of β-cell apoptosis, their insulin levels drop substantially approximately two months later, resembling the pathomechanism of human T2DM [10, 11]. Meanwhile, the control group (ZDF lean) with the dominant allele of the leptin receptor mutation (ZDF Fa/Fa or Fa/fa) does not show any signs of DM. At the initial stage, a hyperinsulinemia is characteristic in ZDF rats.

1.2. The ophthalmological aspects of diabetes mellitus

DM is a chronic metabolic disease with not only a severely impaired carbohydrate metabolism but concomitantly also an impaired lipid and protein turnover due to the complete or relative insulin production deficiency and thus the lack of the insulin effect [12].

The complications of DM can affect almost all structures of the eye. Infections of the eyelids, cornea, and conjunctiva; accommodation disorders; a characteristic "snowflake cataract"; primary open-angle glaucoma; and recurrent injuries of the cornea due to poor wound healing are common. Diabetic neuropathy (DNP) can affect the cranial nerves as well as the ocular muscles, and early on may lead to diabetic keratopathy [13]. Microangiopathy and ischemia can drive the production of various growth factors and thus lead to neovascularization, which may in turn lead to secondary rubeotic glaucoma, both of which have poor visual prognosis. Transient visual disturbances can occur during hyperglycemic episodes due to osmotic thickening of the lens, while permanent visual impairment occurs mostly due to diabetic macular edema (DME) or proliferative diabetic retinopathy (PDR). It is known that DM patients with poor glycemic control develop visually significant cataracts approximately 5 years earlier than average.

1.2.1. Pathophysiology – diabetic neuropathy and microangiopathy in the eye

Impaired glucose metabolism in DM causes an emergence of alternative pathways of carbohydrate turnover (e.g., the sorbitol, hexosamine, or AGE-related pathways) [14]. These together lead to the increased activation of protein kinase C and the accumulation of reactive oxidative and advanced glycation products, which on the one hand directly alter the protein synthesis, while on the other hand increase the cytoplasmic levels of different inflammatory mediators and growth factors (interleukins, vascular endothelial, platelet-derived and insulin-like growth factors etc.) [15].

With the acceleration of protein glycation and cytokine accumulation, morphological and functional damage occurs: increased blood viscosity and platelet adhesion, thickening of the capillary basement membranes, and abnormal endothelial proliferation lead to focal capillary thromboses and later retinal ischemia. Meanwhile, pericyte damage paired with impairment of the endothelial tight junctions and weakening of the capillary walls results in intraretinal hemorrhages as well as to fluid and protein extravasation, leading to further deterioration of the blood supply [16].

The role of diabetic neurodegeneration in the development of DR has been recently explored in more detail. Animal studies have shown histological changes such as amacrine and Müller-cell apoptosis, whereas thickness alterations of the retina or its different layers (RNFL, GCL, IPL) were reported by optical coherence tomography

(OCT) in early stages of DR [17-22]. Early functional changes in humans such as reduced contrast sensitivity or electroretinographic alterations point to a neurodegenerative component of DR before the appearance of the typical diabetic changes [23, 24].

1.2.2. Diabetic retinopathy

Worldwide estimates suggest that after a disease duration of twenty years, 75% of T1DM and 50% of T2DM patients develop at least some form of DR [25]. Other evidence suggests that already after a fifteen-year disease duration, 10% of DM patients experience severe visual impairment, with 2% being legally blind [26].

In Hungary in particular, Tóth et al. described a prevalence of DM (798,300) and DR (160,500) among the Hungarian population over 50 years of age in 2018 [27]. According to their work, the yearly costs in Hungary related to diabetes will rise from 146 million USD (2016) to 168 million USD by 2045, with current annual per-patient costs of almost 200 USD [28].

Characteristic early signs of retinal damage are the microaneurysms, intraretinal bleeding, and microinfarcts caused by the disturbances of the axonal circulation with surrounding focal edema called cotton-wool spots. Later on, due to the increased growth factor production, existing small blood vessels transform increased endothelial proliferation and shunt formation, resulting in intraretinal microvascular abnormalities or retinal neovascularization. This latter sign is a characteristic of the most advanced, sight-threatening stage of DRP, called proliferative diabetic retinopathy. At this stage, the consequent retinal ischemia leads to abnormal vascular proliferation and fibrotic transformation, and hence to the development of vitreous hemorrhages, vitreoretinal traction, and retinal tear or detachment, resulting in the loss of vision.

The severity grading of DR and DME in clinical trials is still based on the Early Treatment Diabetic Retinopathy Study (ETDRS) severity scale that serves as the gold standard, its use has proven to be complicated for everyday practice. A simplified classification of DR and DME based on the ETDRS criteria was developed by the American Academy of Ophthalmology (AAO), called the International Clinical Diabetic Retinopathy Disease/Macular Edema Severity Scale; this allows a rapid

classification with technical requirements that are more suitable for the everyday clinical setting [29].

1.2.3. Diabetic macular edema

Due to the aforementioned impairment of the capillary barrier function in the macula, the extravasation of proteins and lipids may lead to macular edema and the formation of lipid deposits (also called hard exudates). DME can cause severe visual impairment in patients with diabetes and is, in fact, the major cause for vision loss in DM [26]. The stronger adhesion of the ILM to the vitreous limiting membrane may also facilitate DME formation due to vitreoretinal traction [30].

It is important to clarify that DME is not a separate stage of DR, but an independent entity that can manifest at any stage of the disease. The classification of DME by the AAO distinguishes mild, moderate, and severe stages based on the findings observable on dilated funduscopy [29].

1.2.4. Epidemiological, economic, and health system related considerations

The World Health Organization reports that the number of people affected by DM has risen from 108 million to 537 million in the last 40 years, and is predicted to grow further to 643 million by 2030 [31, 32]. The 2021 report of the International Diabetes Federation (IDF) suggest that 75% of adult diabetics come from countries with low or middle income [31]. The health expenditure caused by DM in 2021 was as high as 966 billion dollars worldwide – a 316% increase over the last 15 years [31]. The improvements in healthcare and the lifestyle changes of the last few decades have contributed to DM becoming the number-one cause of preventable blindness among working-age adults. That is, severe vision loss unnecessarily develops in a large number of patients; appropriate treatment alone could lower the risk of moderate vision loss or blindness due to DM by more than 90% [33]. The limited availability of trained human graders and retina specialists is also a major problem throughout the world. As a consequence, because of the growing population automated approaches with less human interaction will inevitably spread over time [34].

1.3. Medical imaging in diabetic retinopathy and maculopathy

The role of medical imaging has become more significant in modern medicine, which comes with an increasing need for expertise in the interpretation of images and in the evaluation of datasets [35, 36]. The retina provides an ideal target for imaging due to the transparent media of the eye, and this advantage is widely exploited in ophthalmology by myriad imaging techniques. Due to space constrains, for the purposes of this thesis we describe only color fundus photography and optical coherence tomography below.

1.3.1. Color fundus photography in diabetes mellitus

The use of color fundus photography has been widely implemented in the diagnosis and documentation of diabetic retinal changes. The hallmark ETDRS study used standard sets of retinal images for the classification of DR and DME, which then led to the development of more applicable grading scales for clinical use [37]. Later, color fundus photography was implemented for the screening of DR and DME with great success through the use of human graders. Initially, multiple images per eye were required for screening, while the use of non-mydriatic, wide-field imaging has helped to simplify this need [38-40].

Nowadays, several different settings of non-mydriatic fundus cameras are commercially available in easy-to-transport and easy-to-use designs. There is neither any special training necessary for the medical personnel, or a need for the patients to undertake an inconvenient and costly imaging session in order to be screened for DR and DME. Additional advantages provided by digital technology include significantly easier storage and delivery of the fundus photos to the reading centers, while on the other hand one can benefit from the advantages of image processing and artificial intelligence (AI), making the method a suitable tool for large-volume DR screening.

Telemedical screening programs, such as those implemented in the United Kingdom or in Nordic countries, can enable the early detection and treatment of DR or even macular edema, and thus substantially reduce the incidence of DR-related vision loss [41].

1.3.2. Optical coherence tomography in diabetes mellitus

OCT enables a micrometer-resolution, three-dimensional, non-invasive imaging of the retina in real-time and has now become the most widely used imaging diagnostic tool in medicine. OCT plays a crucial role in the diagnosis and management of DME by

providing multiple biomarkers beyond thickness measurements [42]. Thanks to OCT image processing through the segmentation of B-Scans, near-histological changes can be detected even in the early stages of DM [43, 44]. With quantitative OCT-analysis, objective structural monitoring can even give valuable information about the disease course and treatment efficacy, which in turn may support therapeutic decisions [45, 46]. Based on differences in the optical density and reflectivity extracted from OCT scans, the image processing algorithms are able to separate the different layers of the retina. This can help not only in the measurement of retinal thickness, but also to more precisely localize retinal changes and to better understand the underlying pathophysiology [47, 48].

The recent introduction of OCT angiography in the daily routine enables the quantitative analysis of retinal microvasculature that can also serve as predictive factor in the prognosis of DME and even in the staging of DR [49].

1.3.3. The automation of retinal image analysis using artificial intelligence

Lately, computer assisted image analysis has rapidly gained importance in the processing of the increasingly complex medical imaging data. Machine Learning (ML) has become an important healthcare tool because of the fast AI evolution in various fields of medicine (e.g., ophthalmology, radiology). Since its introduction in the beginning of the second half of the last century, smaller subsets of AI have been invented and implemented continuously: machine learning, neural networks, and deep learning. It is important to understand this terminology in order to comprehend the various developments in the field. Artificial intelligence is a science of any techniques to build intelligent programs and machines that can solve problems creatively, as humans do. The field of Machine Learning is a subset of AI algorithms, allowing computers to learn automatically from experience without being explicitly programmed to do so [50]. Algorithms that are inspired by the neural structure of the human brain are referred to as artificial neural networks (ANN), whereas algorithms that can combine these neural structures in several layers similarly to the central nervous system are called deep learning (DL) algorithms. (**Figure 1**) gives a graphical explanation of these terms and their relationship with each other.

ML has already led to several clinically relevant applications in the field of ophthalmology, among others automated diagnosis, image segmentation, disease prognosis, and disease prediction [36, 51-55]. ML is particularly useful in ophthalmology due to the vast amount of ocular imaging data available in everyday clinical practice including optical coherence tomography, anterior segment photography, corneal topography and fundus imaging which are of utmost importance in the diagnosis and treatment of conditions like glaucoma, DR, papilledema, age-related macular degeneration and cataract [34, 51].

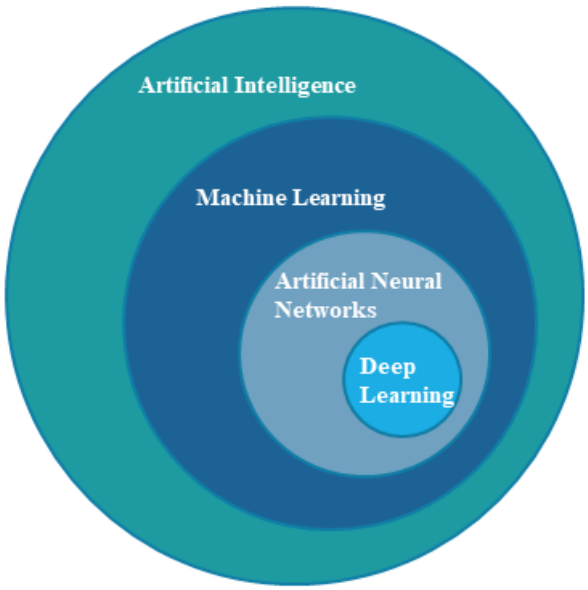

Figure 1. Explanation of the different terms used in the field of artificial intelligence. The detailed explanation can be found in the text.

Several computerized, semi-automated techniques for analysis have been developed for cost efficiency, and to reduce expert workload [56], and the detection of different retinal diseases is now increasingly aided by deep learning (DL) algorithms (e.g., the Bhaktapur Retina Study, a recent study by the Center for Eye Research Australia etc.) [57].

High-quality data play a pivotal part in training new AI/ML models, as they need datasets that are attentively designed and annotated. Furthermore, it is important that such databases contain information on patient characteristics, such as sociodemographic information, the inclusion and exclusion criteria, the labeling process, along with information the labelers themselves [58, 59]. Crowdsourcing has become a new option

for the generation of ground truth data; here, volunteers do the analysis online with or without a charge. Brady et al. recounted using Mechanical Amazon Turk to be an inexpensive and effective method for the rapid identification of ocular diseases like DR or follicular trachoma on photographs [60, 61].

Due to the high amount of imaging data available, multiple uses of AI-driven systems have emerged in the field of Ophthalmology and are developing rapidly. As a result, automated systems using autonomous AI have been recently approved by the FDA for the telemedical screening of the presence/absence of any DR without the need for involving specifically trained personnel [62, 63].

2. OBJECTIVES

In light of the above, we had the following aims in our studies.

1. The use of artificial neural networks to differentiate between healthy and diabetic eyes by structural features of intraretinal layers obtained by OCT imaging

With respect to the underlying relationships between the different structural and optical features of retinal tissue, it could be possible that OCT images could provide more information on the basis of the integration of optical and structural properties. Thus, the images could be used as superior input data to improve diagnostic performance for classification methods. For this reason, we aimed to assess the possibility of training an artificial neural network to distinguish between healthy eyes and eyes of diabetes patients with and without mild diabetic retinopathy using structural data of intraretinal layers obtained by OCT.

2. Detailed histological evaluation of ganglion cells in the retina of ZDF rats

Due to the potential importance of retinal ganglion cells (RGC) in the pathophysiology of early diabetic retinal changes, the contradictory results in other experimental animals [64-66], and the uncertainty of analyzing RGC loss in our former investigations based on the relatively small number of sections, we aimed for a more elaborate histological RGC assessment in the same T2DM model, using three different pan-ganglionic markers.

3. The assessment of the reliability of image quality labeling by graders having different backgrounds

It is of pivotal role to have a satisfactory amount of data to train and validate ML for which correctly labeled ground truth data are required. To model the democratization of the labeling of retinal images, we evaluated the performance of graders with or without medical background in a pilot study for retinal fundus image quality labeling with the help of a special grading tool. It was assessed whether more detailed labeling leads to better reproducibility of results; also, we evaluated the ability to identify poor-quality images. Lastly, we asked graders for feedback so that we could assess their impressions.

3. METHODS

3.1. Training of a Bayesian artificial neural network with OCT images

3.1.1. Patients

One hundred twenty participants (190 eyes) were invited between October 2007 and December 2010 at the Department of Ophthalmology, Semmelweis University, Budapest, Hungary. All Type 1 diabetic patients were invited who had been referred to the comprehensive ophthalmology clinic, and had diabetic retinopathy up to ETDRS level 35 but no macular edema; diabetic patients without retinopathy were also enrolled. Patients over 18 could participate, exclusively, and each subject was asked to sign a written informed consent. Diabetic patients with PDR, clinically significant macular edema, or with anatomic abnormalities that affected the architecture of the macula, e.g., glaucoma, epiretinal membranes, or vitreoretinal traction, were excluded from the study. Healthy controls could be included in the study if they had a best-corrected visual acuity of 20/25 or better, had no present ocular or systematic disease, and a normal-looking macula on contact lens biomicroscopy. Patients who had any medical condition possibly affecting visual function different from T1DM, or medicated treatments that might affect the thickness of the retina, were not included in the study. Furthermore, we excluded individuals from the study who had recent cataract surgery, or had undergone intraocular surgery, as well as patients whose blood sugar levels were unstable, or who had started insulin pump therapy recently.

Thirty-five eyes belonging to 21 study subjects were excluded due to OCT scans of low quality (1) or other diseases that were included in the exclusion criteria (amblyopic (3), chorioretinitis (2), moderate DR (6), no DR (2), epiretinal membrane (1), panretinal photocoagulation (5), pars plana vitrectomy & panretinal photocoagulation (1), pigment epithelial detachment & central serous chorioretinopathy (1), T2DM (8), optic nerve disease (3), and severe DR (2)). We analyzed the remaining 155 eyes belonging to 99 participants, and received 74 healthy eyes in total (34 ± 12 yrs., 52 females, 22 males), 38 eyes with T1DM with no retinopathy (35 ± 10 yrs., 20 females, 18 males), and 43 eyes with mild diabetic retinopathy (MDR, 43 ± 17 yrs., 21 females, 22 males) on biomicroscopy, which we incorporated in the study (**Table 1**).

The research was conducted in accordance with the tenets of the declaration of Helsinki. We obtained Institutional Review Board approval at Semmelweis University as well as at the Miller School of Medicine, University of Miami.

Table 1. Characteristics of the study population

Characteristic	Controls	DM	MDR
Number of Participants	41	29	29
Number of Eyes	74	38	43
Age (years, mean ± SD)	34 ± 12	35 ± 10	43 ± 17
Female, N (% total eyes)	52 (70%)	20 (53%)	21 (49%)
Race (% Caucasian)	100	100	91
Hemoglobin A1c level (%)	-	7.20 ± 0.90	8.51 ± 1.76
DM duration (years, mean ± SD)	-	13 ± 5	22 ± 10
IOP (mmHg, mean ± SD)	-	15.74 ± 1.77	15.09 ± 1.56
BCVA	1.00 ± 0.00	1.00 ± 0.00	0.97 ± 0.06
Total macular thickness	324.36 ± 10.27	316.72 ± 21.56	297.40 ± 21.79

Abbreviations: SD = standard deviation; N = number; DM: diabetic eye without retinopathy; MDR: diabetic eye with mild diabetic retinopathy; IOP = intraocular pressure; BCVA = best corrected visual acuity (67).

3.1.2. Clinical Examination

Enrolled subjects were required to undergo a single comprehensive eye examination which included intraocular pressure (with the Goldmann tonometer) and slit-lamp examination. We performed OCT examination in healthy as well as diabetic eyes with retinopathy and without. An experienced grader obtained and classified fundus images in accordance with the criteria of the ETDRS protocol [68]. Experienced, board-certified graders performed the classification of images unaware of clinical data or the OCT findings. Additionally, a blood test measuring hemoglobin A1c level was carried out at this visit in the case of diabetic patients who had no past glycemic control. After the first visit or during the time of the research no additional tests had to be done.

3.1.3. OCT system and examination protocol

The OCT system (Stratus OCT, Carl Zeiss Meditec, Dublin, California) that we applied in this research uses a broadband light source with an output power of 1 mW at the central wavelength of 820 nm with a 25 nm bandwidth. The light source provides 12μm axial resolution in free space, which determines the system's imaging axial resolution. A cross-sectional image is obtained by combining axial reflectance while the sample is being laterally scanned.

All included Stratus OCT scans were gained with the help of the macular thickness map protocol, which comprises six radial scan lines that are centered on the fovea; every one of them has a 6 mm transverse length. So as to get the best image quality, optimization and focusing settings were controlled. The scans were only accepted when the signal strength was over 6 (preferably 9–10). We repeated scans with foveal decentration. For each case, macular radial line scans of the retina were recorded on disc with the help of the export feature of the Stratus OCT device and were analyzed via custom-built software [69].

3.1.4. OCT image segmentation and data extraction (OCTRIMA)

In our examinations, the OCT scans were processed with "OCT Retinal Image Analysis" (OCTRIMA), a Matlab interface image analysis program developed by Cabrera et Al. [69, 70] which also enables the measurement of the thickness, reflectivity, and optical density of the retinal layers (**Figure 2**).

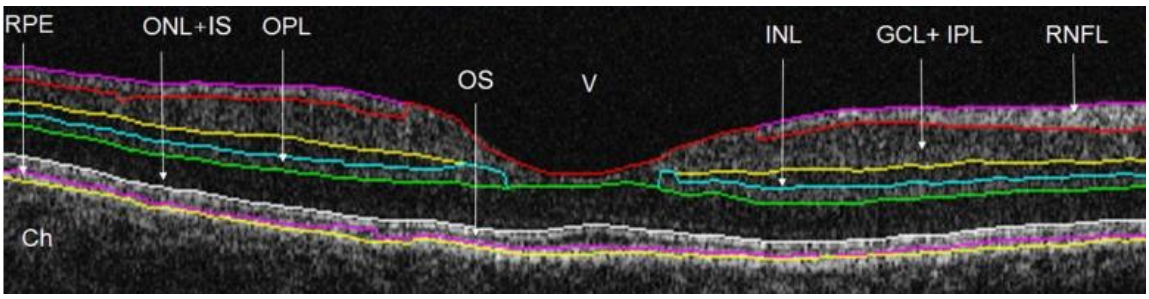

Figure 2. Macular image segmentation using OCTRIMA. The image of a healthy macula scanned by Stratus OCT and processed with OCTRIMA. Abbreviations: Ch, choroid; GCL+IPL, ganglion cell layer and inner plexiform layer complex; INL, inner nuclear layer; ONL+IS, combined outer nuclear layer and inner segment of photoreceptors; OS, outer segment of photoreceptors; OPL, outer plexiform layer; RNFL, retinal nerve fiber layer; RPE, retinal pigment epithelial layer; V, vitreous [70].

As it is the case in some Fourier-domain OCT systems, OCTRIMA too calculates the total thickness of the retina between the inner boundary of the second hyperreflective band and the ILM, which has been attributed to the OS/RPE junction in accordance with histological and previous OCT studies [71, 72]. Six cellular layers of the retina were segmented on OCT images on the basis of their optical densities: the RNFL, GCL + IPL complex, the INL, the OPL, the ONL + IS, OS and the RPE (**Figure 2**) [69].

In addition to thickness measurements, structural and optical measurements were obtained with the help of features that were locally measured for each intraretinal layer. Image processing and the calculation of diagnostic parameters were programmed in Matlab 7.0. We divided the macular region into distinct regions (**Figure 3**). The foveola area is the central disc with a 0.35 mm diameter. The rest of the rings are the fovea, parafoveal, and perifoveal areas; their diameters are 1.85, 2.85, and 5.85 mm, respectively. As an area that is 1 mm in diameter is too extended for the foveola region thickness, which is merely about 0.35 mm in diameter, the custom-built map makes it possible to collect more precise information around the foveola region in comparison with the ETDRS thickness map. Furthermore, in this method, no interpolation is used.

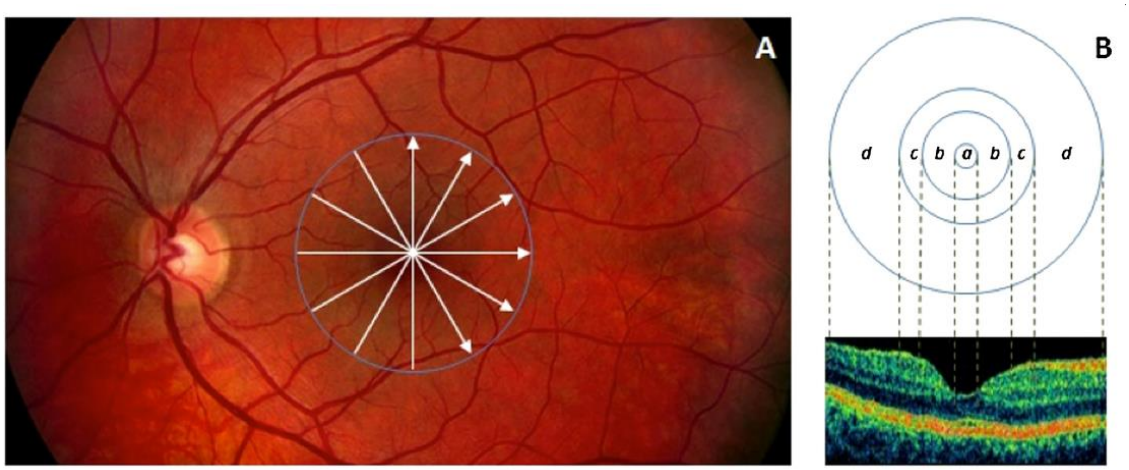

Figure 3. Custom-built method showing macular sectors. A) Fundus image of a healthy eye showing the Stratus OCT's radial lines protocol. B) Regions shown are: foveola (a) with a diameter of 0.35 mm, foveal region (b**)** with a diameter of 1.85 mm, parafoveal region (c) with a diameter of 2.85 mm and perifoveal (d) region with a diameter of 5.85 mm (67).

In addition to measurements of thickness, we extracted optical and structural properties from OCT-based images and used them to classify healthy and diabetic eyes showing

and not showing retinopathy. The parameters that could best distinguish between diabetic eyes and healthy ones, as previous research revealed in statistical and receiver operating characteristic analyses [73], were assessed and validated by artificial neural networks using a Bayesian radial basis function.

3.1.5. Training of a Bayesian basis function network and model testing

Our ANN classifier was composed of an ensemble of two input neurons with a Bayesian radial basis function and one output neuron. As a consequence, we have two features for each candidate intraretinal layer (input parameters) which are put into the ANN so as to estimate one output feature in each of the classification tests. We implemented the ANNs in Matlab 7.0 (MathWorks, Natick, Massachusetts) with the help of Markov chain Monte Carlo algorithms.

To distinguish between diabetic eyes and healthy ones we performed various training and classification tasks. In particular, we chose structural parameters of intraretinal layers as the input and output features for the Bayesian radial basis function networks which would distinguish between MDR, DM, and healthy eyes. As it is indicated in earlier research [74], thickness measurement (TH) and fractal dimension (FD) showed superiority over other parameters in discriminating between MDR, healthy, and DM eyes. Consequently, we used these two optimum parameters for the input and output values that are needed in the training task of Bayesian radial basis function networks. Next, we applied trained Bayesian radial basis function networks for the classification of the combined test subjects (eliminating the training subjects). In order to examine the possible relationships between diseases of the retina in diabetic individuals and target features, the training task was first performed with the help of a part of the data and various target features. Next, we carried out classification tasks to get the optimum arrangement over the allowed models' set. In addition, we used the performance of the classification test to assess the sizing of training dataset in the development of the ANN scheme. Consequently, we explored various sizes of the training set and compared the results we obtained.

We first examined the possible relationships between the alterations of the retina in diabetic individuals and the target features. Specifically, we randomly selected 20 healthy eyes, out of 74 eyes in the control group, in order to train the Bayesian radial

basis function network (Test 1). We used different target features which had been extracted from all of the intraretinal layers for the training of the Bayesian radial basis function network and for the classification of 43 MDR eyes using the rest of the healthy eyes (54 eyes). In this test, the feasibility of the method was evaluated and we determined the best intraretinal layer parameters that could be predicted and used to distinguish between MDR eyes and healthy ones.

Secondly, model testing of the earlier trial was carried out by examining various sizes of the training data subset (Test 2). For this, we used subsets with 20, 30, and 40 healthy eyes to train the Bayesian ANN, and we compared the results.

Next, we attempted to distinguish between DM and MDR eyes (Test 3). In accordance with the earlier test, we randomly selected 20 MDR eyes from the 43 MDR eyes for the training of the Bayesian radial basis function network with the TH and FD as the input and target features. After that, we used the trained Bayesian radial basis function network for the classification of the remaining 23 MDR eyes and 38 DM eyes.

The performance of the proposed methodology was assessed with the help of sensitivity and specificity as figures of merit. We calculated the results for true positive (TP), false negative (FN), true negative (TN), false positive (FP), and positive predictive value (PPV) to evaluate the classification performance of the ANN and the diagnostic capability of the incorporated OCT parameters.

3.2. Histological analysis

3.2.1. Animal handling

All procedures conducted in our research were carried out in accordance with the statement of the Association for Research in Vision and Ophthalmology for the Use of Animals in Ophthalmic and Vision Research. Our research was accepted by the Ethics Committee for Animal Experimentation of Semmelweis University and by the Animal Health and Animal Welfare Directorate of the National Food Chain Safety Office of the Hungarian State (number of approval: 22.1/1162/3/2010).

Our trials were performed on ZDF inbred rats, which were provided by Charles River Laboratories (Sulzfeld, Germany). A part of the results coming from the same trial have already been published [66]. Six-week-old ZDF rats (n = 8) and ZDF lean controls (n = 8) arrived to our laboratory; they were kept in a room with a constant temperature of22

± 2 °C, and were subjected to 12–12 h alternating light-dark cycles. Water and food were provided ad libitum. Their body weights as well as blood glucose levels (Accu-Chek ® Sensor, Roche Inc., Mannheim, Germany) were measured at regular intervals during the whole period of observation. The specimens were euthanized at 32 weeks of age, after they had undergone a range of invasive hemodynamic measurements which had been performed in general anesthesia [75]. In order to remove erythrocytes from tissues, we perfused in vivo 40 ml of oxygenated Ringer solution (37°C, 8 ml/min); after this, the specimens were decapitated. The removed eyes were then placed in fixative within 10 minutes of euthanasia [76].

3.2.2. Tissue preparation and immunohistochemistry

We oriented, removed, and cut the eyes at the ora serrata. We separated the vitreous body, lens and cornea, and the remaining eyecup was fixated in 4% paraformaldehyde diluted in 0.1 M phosphate buffer (PB, pH 7.4) for a period of two hours at room temperature. After the fixation procedure, we rinsed the eyecups multiple times with 0.1 M PB. We applied cryoprotection (in 30% sucrose diluted in 0.1MPB) overnight at 4 °C; next, the eyecups were immersed in tissue-embedding medium (Shandon Cryomatrix, Thermo Scientific, UK). 20-µm-thick cryosections were cut vertically and subsequently stored at −20 °C until use.

Before immunocytochemistry, we blocked all sections in a solution of 0.4 % Triton-X100 (Sigma-Aldrich, Budapest, Hungary) containing 1 % bovine serum albumin in 0.1 M phosphate buffered saline (PBS, pH 7.44). All the primary antibodies that were used were diluted in the same solution, too. Sections were co-labeled using three different markers (Brn-3a, NeuN, and RBPMS), which have been proved to recognize most ganglion cells [77-80]. Details in connection with the primary antibodies we used are provided in **Table 2**. We used three antibodies for 12 hours consecutively with continuous agitation; rinsing steps were repeated in between (PBS, 10 × 10 minutes). Next, the bound primary antibodies were visualized with the help of species-specific fluorescent dyes (Alexa 488 and Alexa 555 conjugates, 1:200, Thermo Fischer Scientific, Waltham, MA) or as for the RBPMS antibodies, biotinylated donkey anti-rabbit (A16039, Thermo Fischer Scientific, Waltham, MA) and streptavidin conjugated Alexa 633 marker. Species-specific Alexa-conjugated secondary antibodies were used

for the detection of the bound antisera at room temperature for 2 hours (Alexa-488 or Alexa-594 conjugates, 1:200, Life Technologies, Carlsbad, CA, USA). We used samples without adding the primary antibodies as negative controls. The nuclei of cells were stained with 4,6-diamidino-2-phenylindole (DAPI, Sigma-Aldrich Kft, Budapest, Hungary).

Table 2. Primary antibodies used in our experiments (76).

Antibodies	Source	Dilution	Host and type	Labelling pattern	Reference
Brn-3a #SC-31984	Santa Cruz Biotechnology Inc., Heidelberg, Germany	1:500	goat polyclonal	retinal ganglion cells	(77)
NeuN Clone:A60 #MAB377	Merck Kft., Budapest, Hungary	1:200	mouse monoclonal	most retinal ganglion cells, some amacrine cells, displaced amacrine cells	(81)
RNA Binding Protein with Multiple Splicing (RBPMS)	Generous donation of Natik Piri, Jules Stein Eye Institute, UCLA, CA, USA	1:500	rabbit polyclonal	retinal ganglion cells	(79)

Additionally, to determine the count of apoptotic cells, we used terminal deoxynucleotidyl transferase deoxyuridine triphosphate nick end labeling (TUNEL, In situ Cell Death Detection Kit, Fluorescein; Roche Diagnostics, Mannheim, Germany) assay. As negative controls, sections incubated without the terminal transferase enzyme were used; positive control sections were pre-incubated with DNAse I before the TUNEL reaction was performed. We counted apoptotic cells in the GCL on complete vertical sections of the retina with the help of terminal deoxynucleotidyl transferase deoxyuridine triphosphate nick end labeling (TUNEL, In situ Cell Death Detection Kit, Fluorescein; Roche Diagnostics, Mannheim, Germany) following the manufacturer's recommendations.

In our research, we used only a few sections to examine the staining features of the antibodies and to evaluate the number of TUNEL positive elements in the GCL. In the

whole of the study, we used only complete vertical sections prepared through the optic nerve of diabetic (n = 4) as well as lean (n = 4) animals, with 4 sections of each specimen for the triple ganglion cell immunohistochemistry as well as for the TUNEL reaction. The majority of the antibodies we used had been previously examined and validated in murine retinas by our research group [19, 65, 82]. Cell counting was carried out on 20 μm thick vertical sections (n = 4 sections from each specimen) obtained from diabetic (n = 4) as well as lean (n = 4) rats. For the purpose of cell counting, we only selected the sections that were crossing the optic nerve head. In the case of ganglion cells (Brn-3a, TUNEL) we counted the total number of the stained cells in each section.

3.2.3. Imaging and statistical analysis

To test triple RGC labeling and for the purpose of quantifying TUNEL reactions, we used a Zeiss LSM 780 Confocal System coupled to a Zeiss Axio Imager upright microsope (Carl Zeiss Meditec AG, Oberkochen, Germany) with a 40x objective.
Our results were analyzed by two-group exact randomization test and expressed as mean ± SD (standard deviation). Also, normal distribution was examined using the Shapiro–Wilks method.

3.3. Fundus image quality labeling and grader performance analysis

3.3.1. Data collection

We chose color fundus photographs from 18,145 color fundus images in total, which were meant to be used for the prospective training of an AI-based algorithm for the purpose of image quality grading. The color fundus images were selected from three datasets: the dataset by Tao et al. [83], the EyePacs dataset [84], and a dataset containing 984 color fundus images, which we had obtained from the Bascom Palmer Eye Institute. These images were acquired with different fundus cameras.
The study was carried out in accordance with the guidelines of the Declaration of Helsinki; for the study, ethics approval was obtained from the ethics committee of the University of Miami. The images were gathered with the consent of the participants and were de-identified in accordance with local regulations (e.g., the Health Insurance Portability and Accountability Act).

3.3.2. Image grading

We developed a system for image classification on the basis of previous research by Zapata et al., Fleming et al., and Gulshan et al., as well as on the EyePACS image quality grading system [84-87]. In summary, we used four criteria for the definition of image quality: focus, illumination, image field definition and artifacts. On the basis of these criteria, we created four groups: excellent (E, all criteria sufficiently met), good (G, maximum 2 criteria not met), adequate (A, 3-4 criteria not met, but the retina can be recognized) and insufficient for grading (I, where no retina can be detected on over 50% of the image; no third-generation branches of the vasculature of the retina can be detected one disc diameter from the optic nerve head and the fovea). For each of the image quality groups, a representative image along with its labels was shown on **Figure 4.**

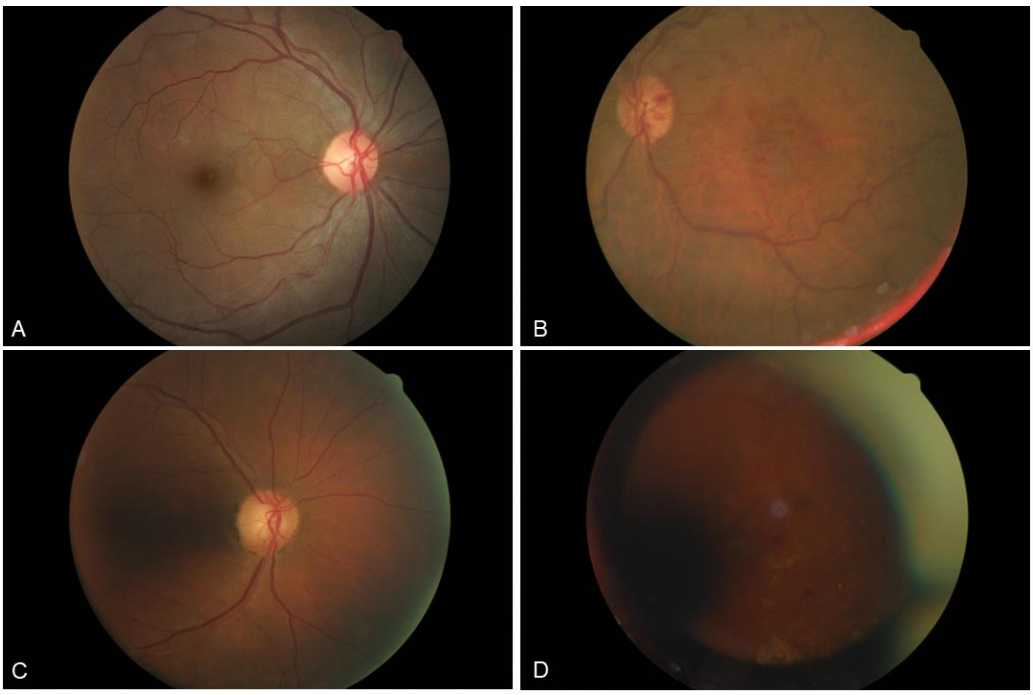

Figure 4. Representative color fundus images from the Excellent (A), Good (B), Adequate (C) and Insufficient for grading (D) categories. Image 1B meets criteria for "Good" because of the image field definition (decentered image) and peripheral artifacts; 1C is identified as Adequate because of its poor illumination, off focus, and insufficient image field definition (the image does not include enough of the retina temporal to the fovea). Image 1D qualifies as Insufficient because it does not show the optic nerve head or the third-generation vessel branches around the macula; this makes it impossible to identify the retinal changes that are characteristic of diabetic retinopathy [88].

Two hundred images were randomly selected out of a set of 18,145 expert-labeled images; from each group, fifty images were chosen. The images had been labeled earlier regarding the quality of the images by two experts, and were used as the basis for the analysis on the ground of the standards defined above. The experts included a board-certified ophthalmologist (KLLF) who had experience retinal imaging, and a board-certified senior retina specialist (GMS) with experience in retinal image grading in the field of the telemedical screening of diabetic retinopathy. When there was disagreement, GMS's decision was used as a reference.

We developed a tkinter-based graphical user interface (GUI) tool in Python programming language, gaining ideas from the number of open-source tools available (https://docs.python.org/3/library/tkinter.html, last accessed 11 July, 2021), with the main intention to develop a simple, on-prem image annotation tool. The tool also allowed for the measuring of the time of the grading in the case of each image shown in 900x1000 pixel resolution; zooming was not possible.

In this study, all the images were assessed by 8 volunteers, 4 of them with a medical background (3 ophthalmologists and 1 optometrist, 26-45 years of age – group M) and 4 without a medical background (2 computer scientists, 1 lawyer, and 1 teacher, 26-60 years of age – group NM). Every volunteer had computer skills of at least intermediate level computer skills working with a PC on a daily basis. Before the grading took place, the participants were given a tutorial with an oral explanation detailing the task and a PDF document which described the anatomy of the retina, along with the grading system using sample images with examples of various artifacts, and a description of the GUI. All the volunteers were allowed to use the supporting PDF document while grading the images. The fundus photographs were shown to the graders in the same, random order. We recorded the time that was necessary for the grading in the case of each volunteer.

To increase grading objectivity, our volunteers were requested to run a second round of grading with the same tool, but this time using 14 predefined labels (**Table 3**). With these labels we generated the aforementioned four image quality groups from excellent to insufficient. Written feedback was collected from the graders upon completion of the second round.

Table 3. Grading labels used for the objective grading round.

Grading categories	Labels used in the objective grading round
Focus	Optimal / Unsharp
Illumination	Optimal / Too dark / Too light
Image field definition	Optimal / Missing Macula / Missing Optic disc
Artefacts	No artefacts / Small pupil / Dust spots / Lash artefacts / Camera artefacts / Arc defects

To reduce the inherent subjectivity of our study, our volunteers were asked to carry out a second round of grading; predefined labels assigned to each category were used. In the second round, the four categories were compiled in a similar way to the first round of grading [88].

3.3.3. Statistical analysis

For the comparison of the times necessary for the grading in the four categories, the medians and interquartile range (IQR)were used because of the limited number of graders in both the M and NM groups.

The inter-rater agreement was assessed by Cohen's weighted kappa in both the original and the more objective grading rounds using the 4 categories of our original grading system (E/G/A/I), as well as after merging Excellent and Good categories [(E+G)/A/I]. In order to evaluate the agreement in choosing images of poor quality, in both rounds, we calculated Cohen's weighted kappa with merged groups E and G vs. A and I. The kappa values are displayed as medians (IQR) altogether as well as in the groups with different previous medical training (M, NM). The statistical analysis was performed with SPSS 28 (SPSS Inc, Chicago, IL).

4. RESULTS

4.1. *The evaluation of the potential of structural features of intraretinal layers extracted from optical coherence tomography images for the training of artificial neural networks to differentiate between healthy and diabetic eyes*

We analyzed 930 OCT images which we had acquired from 155 eligible eyes belonging to 99 participants. The clinical and demographic backgrounds of the participants of the study are described in **Table 1**.

4.1.1. Classification testing using different input parameters to identify healthy eyes – Test 1

In this classification test, we examined the probability of the subject's eye being healthy (diagnostic condition). **Table 4** indicates displays the specificity, sensitivity and predictive values which were obtained when training the Bayesian radial basis function network with the help of the thickness (TH) and fractal dimension (FD).

Table 4. Classification performance results obtained in Test 1

TH vs. FD	RNFL (eye/scans)	GCL + IPL (eye/scans)	INL (eye/scans)	OPL (eye/scans)	ONL + IS (eye/scans)	OS (eye/scans)	RPE (eye/scans)
TP	48/288	49/294	48/288	48/288	48/288	50/300	51/306
FN	6/36	5/30	6/36	6/36	6/36	4/24	3/18
TN	10/60	35/210	23/138	36/216	10/60	9/54	11/66
FP	33/198	8/48	20/120	7/42	33/198	34/204	32/192
PPV	0.59	0.86 *	0.71	0.87 *	0.59	0.60	0.61
Sensitivity	0.89	0.91*	0.89	0.89*	0.89	0.93	0.94
Specificity	0.23	0.81*	0.53	0.84*	0.23	0.21	0.26

* denotes the intraretinal layer for which the sensitivity, specificity and PPV are greater than 80%. Sensitivity, specificity, predictive values (TP, FN, TN, FP) and positive predictive values (PPV) obtained when training the Bayesian radial basis function network using the thickness (TH) and fractal dimension (FD) as the input and target features of the given retinal layers, respectively (67).

According to our results, for the healthy eyes the TP test was in the 48–51 range when we mixed 54 healthy eyes with 43 diabetic eyes showing mild retinopathy (MDR). In particular, TP showed high values for OCT parameters of the GCL + IPL complex, OS,

and RPE (49, 50 and 51, respectively). The positive predictive values indicate that the GCL + IPL complex and OPL parameters are highly sensitive (91% and 89%, respectively) in determining that the subject's eye was indeed healthy. Furthermore, high values for sensitivity, specificity, and PPV (≥0.80) were achieved only for the GCL + IPL complex and OPL parameters. Consequently, it is highly probable (≥80%) that the subject will have a healthy GCL + IPL complex and OPL structure.

4.1.2. Classification testing using different sizes of training datasets – Test 2

During the training of the Bayesian radial basis function network using the thickness and fractal dimension as features, we obtained results which showed that the FN and FP remained at a given sensitivity of ≥ 80% for the parameters of the GCL + IPL complex irrespective of the size of the subset of healthy eyes that were used during the training; FN values remaining for the OPL were found to have slightly decreased with the larger number of healthy eyes used in the training of the ANN. In addition, the TN value for the GCL + IPL complex has not changed. High sensitivity and specificity (≥0.80) with relatively high PPV were indicated both for the GCL + IPL complex and OPL. PPV presented with a slightly declining trend for the GCL + IPL complex and OPL with the greater number of the training subset of healthy eyes, probable explanation would be the consequent reduction in the number of healthy eyes in the testing subset. **Table 5** displays the results after using different sizes of training subsets (20, 30, and 40 eyes).

Table 5. Model testing results after changing the size of the training data set

Size of the training dataset	**20 healthy eyes**		**30 healthy eyes**		**40 healthy eyes**	
TH vs. FD	**GCL + IPL (eye/scans)**	**OPL (eye/scans)**	**GCL + IPL (eye/scans)**	**OPL (eye/scans)**	**GCL + IPL (eye/scans)**	**OPL (eye/scans)**
TP	49/294	48/288	39/234	39/234	29/174	29/174
FN	5/30	6/36	5/30	5/30	5/30	5/30
TN	35/210	36/216	35/210	36/216	35/210	36/216
FP	8/48	7/42	8/48	7/42	8/48	7/42
PPV	0.86	0.87	0.83	0.85	0.78	0.81
Sensitivity	0.91	0.89	0.89	0.89	0.85	0.85
Specificity	0.81	0.84	0.81	0.84	0.81	0.84

Results of sensitivity, specificity, accuracy, predictive values, and positive predictive values gained for the GCL + IPL complex and OPL when training the Bayesian radial base function network with 20, 30, and 40 healthy eyes with the thickness (TH) and fractal dimension (FD) as the input and target features, respectively [67].

4.1.3. Classification testing using different input parameters to identify MDR eyes – Test 3

The results that were observed in Test 3 after training the Bayesian radial basis function network with TH and FD as the input and target features are displayed in **Table 6**. This classification test, we investigated the likelihood of diabetic eyes having MDR (diagnostic condition). In this test we obtained high TP values for the features of the RNFL, GCL + IPL complex, OS and RPE. In addition, RNFL, OS, and RPE presented with a sensitivity, specificity, and PPV of at least 70%. Surprisingly, the features of GCL + IPL complex did only present a PPV of 60%.

Table 6. Classification performance results obtained in Test 3

TH vs. FD	RNFL (eye/scans)	GCL + IPL. (eye/scans)	INL (eye/scans)	OPL (eye/scans)	ONL + IS (eye/scans)	OS (eye/scans)	RPE (eye/scans)
TP	18/108	18/108	15/90	4/24	10/60	18/108	20/120
FN	5/30	5/30	8/48	19/114	13/78	5/30	3/18
TN	30/180	26/156	32/192	28/168	26/162	31/186	33/198
FP	8/48	12/72	6/36	10/60	12/72	7/42	5/30
PPV	0.69	0.60	0.71	0.29	0.45	0.72	0.80*
Sensitivity	0.78	0.78	0.65	0.17	0.43	0.78	0.87*
Specificity	0.79	0.68	0.84	0.74	0.68	0.82	0.87*

* denotes the intraretinal layer for which the sensitivity, specificity, and PPV are greater than 80%. Sensitivity, specificity, predictive values (TP, FN, TN, FP), and positive predictive values (PPV) obtained when training the Bayesian radial basis function network using the thickness (TH) and fractal dimension (FD) as the input and target features, respectively [67].

Overall, the results show an approximately 90% effectiveness of the classifier (PPV values in **Table 5**) in providing an exact prediction of the unknown class (healthy eyes) when distinguishing between healthy eyes and MDR eyes based on the GCL + IPL complex' and OPL's features in the diagnostic test (Test 1). Nevertheless, the classifier could not effectively (~44.5%) make a correct prediction when distinguishing between

DM and MDR eyes using the features of the same intraretinal layers (i.e., GCL + IPL complex and OPL in Test 3 – **Table 6**). It proved to be more effective (PPV ~ 74%) in the prediction of the unknown class (MDR eyes) when DM and MDR eyes were compared with the help of the features of the RNFL, OS, and RPE (Test 3). **Table 7** displays the percentage of correct classifications for the GCL + IPL complex and OPL features in tests 1 and 3.

Table 7. Percentage of correct classifications as a function of eyes used in training and testing in tests 1 and 3 (67).

Intraretinal Layer	Number of eyes used for training		Number of eyes used for testing	Percentage of correct classifications (%)
GC + IPL	Test 1	20 Healthy	97	91
	Test 3	20 MDR	61	42
OPL	Test 1	20 Healthy	97	89
	Test 3	20 MDR	61	47

4.2. *Detailed histological evaluation of ganglion cells in the retina of Zucker Diabetic Fatty rats*

4.2.1. Triple retinal ganglion cell labeling on cryosections

In the study, we used three antibodies for the labeling of the majority of RGCs (**Figure 2**). In accordance with the literature, Brn-3a presented a purely nuclear localization [79]; in addition to labeling the nuclei, NeuN also stained the cytoplasm [89]; and RBPMS positivity was most distinctly observed in the cytoplasm. Most labeled cells in the GCL were stained by all of the antibodies; cells positive for either two or only one of the antibodies were only occasionally found. Additionally to the staining pattern in the GCL, NeuN also identified a numerous smaller cells in the inner nuclear layer (INL – in all likelihood amacrine cells – see arrows in **Figure 2b,f**) that did not co-label with the other two antibodies.

Comparing the control specimens with the diabetic ones, we found no major difference in the intensity of the staining or in the localization or number of the labeled elements with any one of the antibodies that were used. We did, however, detect a notable variation between different retinal regions, mainly in the central retina, bordering the optic nerve head. In some parts, no labeled cells were detected, whereas a large group of

cells was detected only 20–50 μm further away. This phenomenon was evidently detectable in control as well as in diabetic specimens.

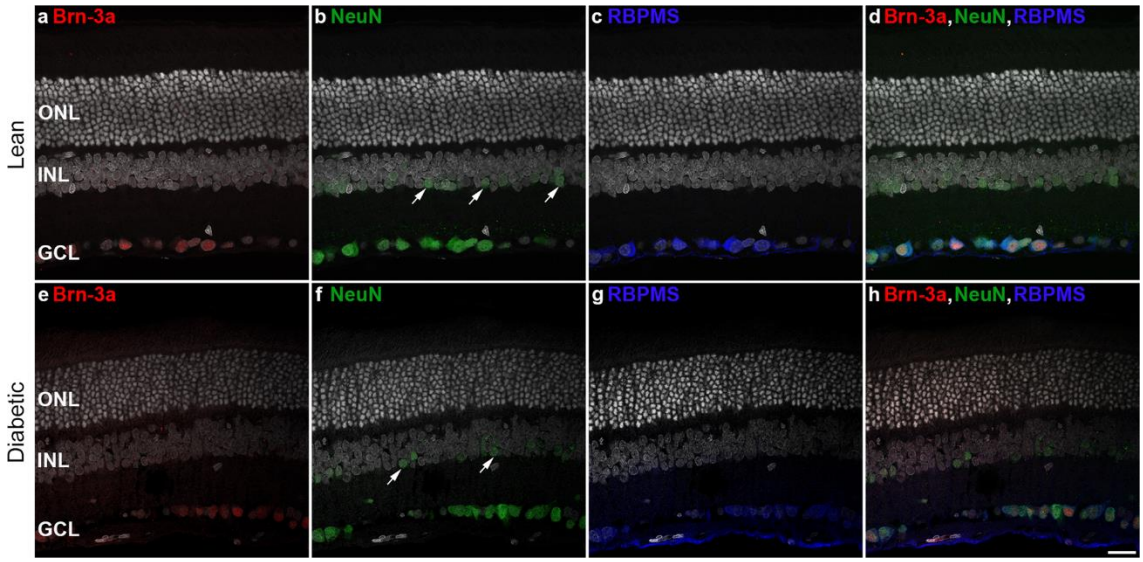

Figure 5. Triple labeling of retinal ganglion cells in retinal cryosections. Representative images of retinal sections of control lean (a–d) and diabetic (e–h) specimens labeled by three different markers Brn-3a (first column - in red), NeuN (second column - in green), and RBPMS (third column – in blue). Merged images are shown in the right column. The vast majority of the RGCs are labeled by all three markers. NeuN also labels a population of cells – most probably amacrine cells – in the INL (arrows on b,f). DAPI is used as a nuclear staining on the sections (in white). ONL: outer nuclear layer, INL: inner nuclear layer, GCL: ganglion cell layer. Bar: 20 μm. [56]

4.2.2. Apoptosis among ganglion cells

In the GCL in each vertical section the mean number of TUNEL positive cells was 1.38 ± 1.54 in control vs. 1.26 ± 1.24 in diabetic specimens. We did not find any significant difference ($p = 0.73$).

4.3. *The assessment of the reliability of image quality labeling among graders with different backgrounds*

4.3.1. Time necessary for the grading task

For the labeling task, the median time (IQR) was 987.8 sec (418.6) in the case of all graders, and 872.9 sec (621.0) vs. 1019.8 sec (479.5) in the M vs. NM groups, respectively. For the first 50 images, the median time necessary (262.8 sec [125.7]) was

slightly longer in comparison with what was needed for the last 50 images (195.8 sec [108.3]). It took graders with a medical background to label the last 50 images in median 28.6 seconds less than the first 50 images. Those graders that had no prior medical training needed in median 38.25 seconds less to label the last 50 images than the first 50.

The median time (IQR) required per single decision in the four categories was 3.35 sec (3.4), 3.8 sec (4.0), 4.0 sec (4.8) and 1.8 sec (2.0) for the E, G, A, and I label, respectively. In the NM group, graders needed longer time to make a single labeling decision in each of the categories compared to the medically trained participants (3.8 vs. 2.4 sec, 4.3 vs. 3.2 sec, 4.6 vs. 3.1 sec, and 2.0 vs. 1.6 sec for the E, G, A, and I in the NM vs. M groups, respectively).

4.3.2. Grader agreement

Cohen´s weighted kappa indicated moderate accordance among the graders when four categories were used (0.564 for all graders and 0.590 vs. 0.554, for the groups M and NM, respectively). The merging of groups E and G lead to the moderate agreement increasing to substantial (0.637 for all graders, and 0.657 vs. 0.627 for the groups M and NM, respectively). There was a further increase in Cohen's weighted kappa when we merged groups E and G vs. A and I (0.665 for all graders, and 0.715 vs. 0.625 for the groups M and NM, respectively) **(Table 8)**.

In the second round of grading, when 14 labels were used, the four categories were compiled analogous to the categories we used in our original grading system (E/G/A/I). Here Cohen's weighted kappa showed a moderate agreement with the use of four categories (0.594 for all of the graders and 0.598 vs 0.568 for the groups M and NM, respectively), and substantial when we merged groups E and G (0.667 for all graders and 0.669 vs 0.612 for the groups M and NM, respectively), while merging groups A and I brought only a minimal increase in agreement all together and among graders with a medical background (0.670 for all graders and 0.708 vs. 0.581, for the groups M and NM, respectively) **(Table 8)**.

Table 8. Inter-rater agreement in the two setups with different image quality category groups.

	4 Image quality grading criteria			14 Predefined labels		
	4 groups	**3 groups**	**2 groups**	**4 groups**	**3 groups**	**2 groups**
Medical	0.590	0.657	0.715	0.598	0.669	0.708
	(0.167)	(0.116)	(0.190)	(0.053)	(0.052)	(0.126)
Non-	0.554	0.627	0.625	0.568	0.612	0.581
medical	(0.176)	(0.147)	(0.175)	(0.085)	(0.107)	(0.127)
Altogether	0.564	0.637	0.665	0.594	0.667	0.670
	(0.163)	(0.096)	(0.178)	(0.60)	(0.80)	(0.151)

Cohens's weighted kappa was determined for the grading using four categories in image quality (Excellent (E)/ Good (G)/ Adequate (A)/ Insufficient (I)); we used 14 labels for the second round of grading. In the second ground, the same four categories were compiled as in the first (E/G/A/I). Cohens's weighted kappa was also calculated with merging groups E and G for both rounds [(E+G)/A/I]. In order to evaluate the agreement when distinguishing between poor quality images in both rounds, Cohen's weighted kappa was determined with two merged groups (E and G vs. A and I). The kappa values are displayed as medians (interquartile range) for all the graders in both groups (medical, non-medical).

4.3.3. The feedback of our graders on the labeling tool

On evaluating the post-task feedback we found that all graders considered the application of the Python image labeling tool simple and grading itself uncomplicated. We must mention, however, that 2 of our 8 graders who had no previous programming experience required help launching the grading tool. They had difficulties during the installation of the package manager of our application, and with command lines to open the application (contrary to the more widespread practice of launching applications by clicking on an icon). As a consequence, we also provided all of our participants with a meticulous "program launching manual" and verbal explanation in the second round of grading, which eliminated these difficulties. Five of the graders considered the size of the images and their resolution rather small for the grading of retinal lesions. All volunteers considered the grading task and both the written and oral tutorials intelligible. During the grading task, no decision fatigue was reported by any of the

graders. Five of the graders reported feeling a detectable improvement in grading with only 200 images and considered the task motivating.

The graders who had medical backgrounds (one optometrist and three ophthalmologists) detected a relatively high number of fundus images having an at least partially missing optic nerve head that was. Two of our graders (one from the M and one from the NM group) wished that the definition of focus and illumination were better defined concerning the visibility of smaller retinal vasculature. Altogether, the feedback from the graders was positive regarding the task and the tool itself.

5. DISCUSSION

Diabetes mellitus puts a large pressure on societies – in both developed and developing countries – as the expenses of diabetes-related ocular pathologies are steadily increasing [32]. In fact, in developed countries one of the main causes of blindness in the population between 20-65 years is diabetes [90, 91]. The sequel to DR and DME is fairly well understood being mostly driven by capillary dropout and resultant retinal ischemia and endothelial damage (which lead to retinal edema and subsequent structural disruption of the retina including loss of photoreceptors) [92, 93].

According to clinical evidence, there is a decrease in the number of retinal ganglion cells (RGCs) prior to visible changes in the retina, before retinopathy can be detected [17, 94]. The decrease in contrast sensitivity [95] and reduced response on electroretinography have been reported in previous studies [96]. Relatively strong clinical evidence with OCT suggests a decline in inner retinal structures, specifically the GCL + IPL complex with some associations of the retinal nerve fiber layer [73, 97, 98].

5.1. The use of artificial neural networks to differentiate between healthy and diabetic eyes by structural changes of the retina obtained by OCT imaging

We presented and assessed a nonlinear prediction technique based on retinal OCT images for early retinopathy detection. Our approach included three phases: first, we performed a segmentation of the OCT images, second, we identified a candidate marker, and finally we formulated a feature set and performed a classification. At the time of our evaluation there were commonly available tools for the quantitative measurement of retinal thickness with OCT, whereas no algorithms have been available for the analysis of the optical characteristics of the retinal tissue. Furthermore, the combination of structural and optical information for the prediction of retinal disruption in diabetes has also not been described before. The predictability of any retinal layer integrity changes – in our example by applying a Bayesian radial basis function network – may be important in the assessment of cellular loss in eyes of patients with diabetes. We could show that these parameters of the ganglion cell-plexiform complex may be useful in the prediction of and could be used for the discrimination between MDR and healthy eyes with the help of the TH/FD pair as the input/target feature in the Bayesian radial basis function network. Fractal dimension provides an estimation of the

roughness of intraretinal structure, and could potentially be used to distinguish eyes with mild non-proliferative retinopathy (NPDR) and eyes from non-diabetic subjects. Our data suggest that the ganglion cells and the OPL might have an increased susceptibility the stage of mild DR. Interestingly, the features of the RNFL, OS, and RPE appeared to be able to estimate structural disintegration of the retina while distinguishing between MDR and DM eyes. This specific result was consistent with previous research that reported alterations in the outer retinal segment during the comparison of the thickness of the macula in diabetic subjects with mild retinopathy and eyes of healthy subjects [68, 99]. These findings could assist in the more precise detection of mild diabetic retinopathy with the help of OCT imaging employed in a screening setting.

We found some limitations to our study employing ANN. Cross-study comparisons were not possible, because there were no studies conducted regarding the changes in retinal thickness and optical tissue properties by the implementation of ANNs. Also, more precise and robust predictions of the classification test performance could have been made using larger sample sizes. Finally, different classification methods are necessary in order to find the best models that can improve the discriminant power of OCT-generated data which are used for clinical decision support. Furthermore, our results had to be confirmed on data provided by Spectral-domain OCT devices because of their higher spatial resolution. However, one must acknowledge that at the time of our study, time-domain Stratus OCT was the most commonly used device world-wide. In the meantime, multiple studies were trying to correlate the observations of the inner and outer retinal changes found with intrinsic ophthalmic imaging (OCT and confocal microscopy) and showed promising results [100, 101]. Still, it is very challenging to align their findings with the supposed metabolic and electrophysiological changes in humans and animal models.

From the second half of the 2010's, there has also been a major development in the ML approaches. With the growing amount and complexity of data and the increasing processing capacity of computers, deep neural networks gained importance, especially deep convolutional neural networks (CNN) in retinal image recognition [36, 102, 103]. In the CNNs there are several "hidden layers of neurons" which allow more abstract data processing and pattern recognition.

Thus, although we employed state-of-the-art methodology at the time of our assessments, deep learning methodologies trained on huge datasets have meanwhile gained substantial importance. Although the exact parameters affecting how these algorithms work are not exactly known due to the "black box effect" (the algorithms do not reveal the features they are observing, only attention maps can be generated in most cases, and it is most possible that these CNNs are using some of the structural or even optical characteristics of the images).

5.2. Detailed histological assessment of ganglion cell changes in Zucker Diabetic Fatty rats

In accordance with our studies employing the Bayesian ANN, there are several clinical studies suggesting a loss of the ganglion cell and IPL complex in diabetes with some involvement of the RNFL as well [73, 97, 98]. These findings are important because they help understand the early pathophysiological changes of the retina which later in severe, sight-threatening complications. In order to assess this in more detail, multiple animal studies were conducted to clarify the involvement of retinal ganglion cells in diabetes and to describe the earliest changes in the retina. Nevertheless, these studies yielded contradictory results, with some studies reporting an involvement of the RGCs [21, 104, 105] and some studies showing no changes [64-66].

According to our work performed in ZDF rats, utilizing retinal sections only and a Brn-3a, NeuN, and RBPMS staining methodology, we could identify photoreceptor degeneration, glial response, and amacrine cell number changes. However, the use of Brn-3a staining was not conclusive of any apoptotic changes in the ganglion cell numbers [66]. In fact, even with the application of additional non- pan-ganglionic markers (NeuN and RBPMS), no morphologically or statistically significant difference could be revealed between diabetic and control ZDF rats, and thus we could not provide evidence for the aforementioned clinical observations. In our model the animals were kept diabetic for a relatively long time of six months, and thus the question remains how this discrepancy arises. According to the 4-year longitudinal results of Sohn et al., there is retinal neurodegeneration preceding the earliest microvascular changes. Their results were confirmed with OCT image analysis and immunohistochemistry in vivo in humans and in rodent models, as well as in a post-mortem human setting [21]. Finding reliable

biomarkers is difficult in the case of DNP; consequently, the clinical observations mentioned above could be considered as clinical substitutes in its diagnosis and therapy.
In our study, we could not show any significant RGC loss or a major change in staining patterns. We could also exclude the possibility of significant IPL pathology resulting in thickness or stratification pattern alterations [76]. According to the above, the clinical observations of GCLC thinning is not the earliest retinal change in diabetes, and thus the outer retinal alterations that we confirmed earlier rather precede any inner retinal pathologies [19, 65, 66, 82]. The latter theory warrants further clinical investigation for the assessment of early diabetic retinal changes.

5.3. *The assessment of the reliability of image quality labeling in the cohort of graders with diverse backgrounds*

The structural retinal alterations in diabetes detectable on either OCT or color fundus images could serve the early detection and classification of diabetic retinopathy, and thus help to prevent diabetic vision loss. Based on this, many computerized, semi-automated analysis techniques are known in the literature that could decrease the amount of work and related expenditure for expert image grading [56]. Simultaneously, deep learning algorithms are increasingly being adopted that can be helpful in the timely diagnosis of various retinal pathologies [57].
The implementation of such DL algorithms requires training on a large set of meticulously and precisely labeled images, and thus the grading performance of the algorithm strongly relies on the quality of the data used for training. Therefore, the labeling step is crucial in obtaining reliable results and is often a source of unnoticed bias in the development of DL-based solutions for screening or diagnostic purposes. According to previous data, following intensive training of 1-2 months, mid-level ophthalmologic personnel or even non-expert, non-medical graders are able to accurately classify photos of the retina with at least a moderate level of DR [106-108]. The process of image labeling in the generation of ground truth can be made more time-efficient through crowdsourcing, where volunteers do an online analysis with or without a charge. Mechanical Amazon Turk is considered to be relatively inexpensive yet still effective to rapidly identify ocular diseases such as follicular trachoma or DR on photographs [60, 61]. In contrast to recent literature describing inter-rater repeatability,

we also examined the time of single decisions and the time for the completion of quality labeling with different complexities, in the hands of graders with or without a background in medicine.

Previous data suggests [60], graders without medical background can grade retinal photographs rapidly and in a cost-effective way. Non-medical graders in our study spent seventeen minutes in median on the grading of 200 images. Based on this, the labeling of 20,000 retinal images should be completed in merely 90 minutes by a total of 20 graders without any background in ophthalmology. Medically trained labelers can potentially achieve better results; nevertheless, in this case reproducibility and specificity/sensitivity would also need to be evaluated using images from different pools [60].

We developed our python-based grading tool also to assess general image quality with the help of human labelers. We also wanted to assess if the delegation of labeling to people without medical knowledge could be of any disadvantage.

We employed a set of fundus images that had been taken by different fundus cameras, thus representing a real-life setting where image quality labeling does not depend on the device used for imaging, serving as a further strength of our work.

AI together with its advantages as well as drawbacks will become accessible to a large number of people. The importance of crowdsourcing is on the rise in various projects that utilize human intelligence. Our work is significant in that it may provide some help on obtaining reliable ground truth data – even with the help of incompletely trained volunteers – for the training of deep learning algorithms in the future. Our results imply that fewer labels and grading categories can be sufficient to achieve this goal. Besides, such a simple tool can help to solve the well-known problem with images of poor quality that is present in all public repositories (such as EyePACS and MRL Eye) and also in various smaller databases of various institutions. These images hinder not only the grading but also the training of AI-based algorithms. Our solution could be easily implemented to pinpoint poor quality images and thus improve grading efficiency, even by simply involving “citizen scientists”. Our aim is to utilize our tool to further label fundus images aimed for the automated assessment of image quality and diabetic

DOI:10.14753/SE.2023.2807

retinopathy grading. We hope that our application will also aid the advancement of other deep learning algorithms in the field.

DOI:10.14753/SE.2023.2807

6. CONCLUSIONS

In our work we investigated different aspects of diabetic retinal changes in vivo, both histologically and using clinical imaging methods.

1. We could show that by using a Bayesian ANN with retinal OCT parameters as an input feature, the distinction between healthy and diabetic eyes without retinal changes (DM) and with mild retinopathy (MDR) is feasible.

2. In fact, the fractal dimension of the GCL + IPL complex and OPL which had been predicted by the Bayesian radial basis function network could distinguish eyes with mild NPDR from healthy eyes. Additionally, the thickness and fractal dimension of the RNFL, OS, and RPE seem to be promising biomarkers for the classification of eyes in diabetic patients with or without any signs of mild NPDR.

3. In contrast to this, our work in a ZDF rat model of type 2 diabetes could not confirm any direct ganglion cell loss which is suggestive of early retinal changes happening elsewhere in the retina, most possibly in the outer retina as proposed by other studies. This is in line with the additional parameters identified in our clinical study (namely, the OS and RPE) and warrants further investigation.

4. The retinal funduscopic features are equally important for the detection of diabetic retinal changes as the structural information derived from OCT. We could show that for the ground truth generation of databases that enable the training of AI algorithms, high agreement level can be achieved even by a very short training and a small number of fundus images, despite the lack of medical background.

5. Our results underline the importance of a simple grading scheme in this scenario, as it might be difficult to appreciate fine image quality features when utilizing robust deep learning techniques.

6. Our methodology has been proven to be user-friendly and well perceived by participants. It can efficiently serve the generation of training datasets of AI algorithms for the robust distinction of poor-quality images that are insufficient for screening.

DOI:10.14753/SE.2023.2807

7. SUMMARY

Visual impairment due to diabetes mellitus (DM) poses a huge burden on societies all over the world. The better understanding of diabetes-related retinal changes and their early detection is of pivotal importance in the prevention and efficient treatment of diabetic eye complications. The diagnosis of these alterations is mostly based on optical coherence tomography (OCT) imaging for diabetic macular edema and color fundus photography for diabetic retinopathy (DR). The vast amount of imaging data necessary for population-based screening calls for action to increase efficiency through the implementation of resource saving tools based, among others, on advanced artificial (AI) intelligence-driven technologies.

In our current work, we aimed to combine different approaches to address this problem. First, we investigated the early diabetes-related OCT markers that could identify early diabetic retinal pathology using artificial intelligence before any structural changes develop. As a second step and based in part on these results, we looked at ganglion cell changes in an animal model of type 2 diabetes. Finally, we assessed the aspects of image quality labeling of color fundus photographs from diabetic subjects using a Python-based tool under different conditions, through the employment of graders with or without medical backgrounds.

We found that a Bayesian artificial neural network with features extracted from OCT data could potentially discriminate between healthy eyes and eyes with or without mild DRP by using data from the ganglion cell and inner plexiform layer complex. In contrast to this, we could not confirm any ganglion cell changes in the ZDF model of Type 2 diabetes, which suggests that the clinical observation of inner retinal changes might be a more chronic sequel in diabetes. Finally, the third part of our work shows promise that even “citizen scientists” undergoing very brief training could achieve high levels of agreement in the labeling of color fundus photographs using simple grading systems and only a few categories. This, in turn, can provide better ground truth data within a short time frame and employ significantly fewer resources for the training of deep learning-based algorithms.

In summary, our work based on clinical imaging and animal histological data might contribute to a better understanding and earlier detection of diabetic retinal pathology.

8. REFERENCES

1. Kolb H. Simple Anatomy of the Retina. In:Kolb H, Fernandez E ,Nelson R (szerk.), Webvision: The Organization of the Retina and Visual System. Salt Lake City (UT), 1995.
2. Bringmann A, Wiedemann P. (2012) Muller glial cells in retinal disease. Ophthalmologica, 227: 1-19.
3. Ahnelt PK. (1998) The photoreceptor mosaic. Eye (Lond), 12 (Pt 3b): 531-540.
4. Mollon JD, Regan BC, Bowmaker JK. (1998) What is the function of the cone-rich rim of the retina? Eye (Lond), 12 (Pt 3b): 548-552.
5. Curcio CA, Sloan KR, Kalina RE, Hendrickson AE. (1990) Human photoreceptor topography. J Comp Neurol, 292: 497-523.
6. Lukáts Á. (2004) Photopigment coexpression in mammals: compartive and developmental aspects. Ph. D. Thesis. In: Department of Human Morphology and Developmental Biology, Semmelweis University, Budapest
7. King AJ. (2012) The use of animal models in diabetes research. Br J Pharmacol, 166: 877-894.
8. Phillips MS, Liu Q, Hammond HA, Dugan V, Hey PJ, Caskey CJ, Hess JF. (1996) Leptin receptor missense mutation in the fatty Zucker rat. Nat Genet, 13: 18-19.
9. Peterson RG, Little LA, Neel MA. (1990) WKY Fatty Rat as a Model of Obesity and Non-insulin-dependent Diabetes Mellitus. ILAR J, 32: 13-15.
10. Sparks JD, Phung TL, Bolognino M, Cianci J, Khurana R, Peterson RG, Sowden MP, Corsetti JP, Sparks CE. (1998) Lipoprotein alterations in 10- and 20-week-old Zucker diabetic fatty rats: hyperinsulinemic versus insulinopenic hyperglycemia. Metabolism, 47: 1315-1324.
11. Finegood DT, McArthur MD, Kojwang D, Thomas MJ, Topp BG, Leonard T, Buckingham RE. (2001) Beta-cell mass dynamics in Zucker diabetic fatty rats. Rosiglitazone prevents the rise in net cell death. Diabetes, 50: 1021-1029.
12. Gaál Zs GL, Hidvégi T, Jermendy Gy, Kempler P, Winkler G, Wittmann I, (ed. Jermendy Gy). (2017) Egészségügyi szakmai irányelv – A diabetes mellitus

kórismézéséről, a cukorbetegek antihyperglykaemiás kezeléséről és gondozásáról felnőttkorban. 25: 3-77

13. Friend J, Thoft RA. (1984) The diabetic cornea. Int Ophthalmol Clin, 24: 111-123.
14. Davidson MB, Bate G, Kirkpatrick P. (2005) Exenatide. Nat Rev Drug Discov, 4: 713-714.
15. Brownlee M. (2001) Biochemistry and molecular cell biology of diabetic complications. Nature, 414: 813-820.
16. Tabandeh HG, M. F. The Retina in Systemic Disease: A Color Manual of Ophthalmoscopy. Thieme Medical Publishers, New York, 2009: 21-36
17. Barber AJ. (2003) A new view of diabetic retinopathy: a neurodegenerative disease of the eye. Prog Neuropsychopharmacol Biol Psychiatry, 27: 283-290.
18. Gastinger MJ, Singh RS, Barber AJ. (2006) Loss of cholinergic and dopaminergic amacrine cells in streptozotocin-diabetic rat and Ins2Akita-diabetic mouse retinas. Invest Ophthalmol Vis Sci, 47: 3143-3150.
19. Enzsoly A, Szabo A, Kantor O, David C, Szalay P, Szabo K, Szel A, Nemeth J, Lukats A. (2014) Pathologic alterations of the outer retina in streptozotocin-induced diabetes. Invest Ophthalmol Vis Sci, 55: 3686-3699.
20. Pardue MT, Barnes CS, Kim MK, Aung MH, Amarnath R, Olson DE, Thule PM. (2014) Rodent Hyperglycemia-Induced Inner Retinal Deficits are Mirrored in Human Diabetes. Transl Vis Sci Technol, 3: 6.
21. Sohn EH, van Dijk HW, Jiao C, Kok PH, Jeong W, Demirkaya N, Garmager A, Wit F, Kucukevcilioglu M, van Velthoven ME, DeVries JH, Mullins RF, Kuehn MH, Schlingemann RO, Sonka M, Verbraak FD, Abramoff MD. (2016) Retinal neurodegeneration may precede microvascular changes characteristic of diabetic retinopathy in diabetes mellitus. Proc Natl Acad Sci U S A, 113: E2655-2664.
22. Verbraak FD. (2014) Neuroretinal degeneration in relation to vasculopathy in diabetes. Diabetes, 63: 3590-3592.
23. Luu CD, Szental JA, Lee SY, Lavanya R, Wong TY. (2010) Correlation between retinal oscillatory potentials and retinal vascular caliber in type 2 diabetes. Invest Ophthalmol Vis Sci, 51: 482-486.

24. Feitosa-Santana C, Paramei GV, Nishi M, Gualtieri M, Costa MF, Ventura DF. (2010) Color vision impairment in type 2 diabetes assessed by the D-15d test and the Cambridge Colour Test. Ophthalmic Physiol Opt, 30: 717-723.
25. Klein R, Klein BE, Moss SE, Davis MD, DeMets DL. (1984) The Wisconsin epidemiologic study of diabetic retinopathy. III. Prevalence and risk of diabetic retinopathy when age at diagnosis is 30 or more years. Arch Ophthalmol, 102: 527-532.
26. Varma R, Torres M, Pena F, Klein R, Azen SP, Los Angeles Latino Eye Study G. (2004) Prevalence of diabetic retinopathy in adult Latinos: the Los Angeles Latino eye study. Ophthalmology, 111: 1298-1306.
27. Toth G, Nagy ZZ, Nemeth J. (2021) Model-based economic burden of diabetic retinopathy in Hungary. Orv Hetil, 162: 298-305.
28. Toth G, Limburg H, Szabo D, Sandor GL, Nagy ZZ, Nemeth J. (2021) Rapid assessment of avoidable blindness-based healthcare costs of diabetic retinopathy in Hungary and its projection for the year 2045. Br J Ophthalmol, 105: 1116-1120.
29. Wilkinson CP, Ferris FL, 3rd, Klein RE, Lee PP, Agardh CD, Davis M, Dills D, Kampik A, Pararajasegaram R, Verdaguer JT, Global Diabetic Retinopathy Project G. (2003) Proposed international clinical diabetic retinopathy and diabetic macular edema disease severity scales. Ophthalmology, 110: 1677-1682.
30. Somfai GM. (2008) Clinical and laboratory assessment of diabetic microvascular complications. Ph. D. Thesis. In: Department of Ophthalmology, Semmelweis University, Budapest
31. International Diabetes Federation. Diabetes Atlas. (10th Edition): Brussels. Belgium; 2022. https://diabetesatlas.org/ (last accessed on July the 28th 2022)
32. World Health Organization. Global Report on diabetes 2021. https://www.who.int/news-room/fact-sheets/detail/diabetes (last accessed on July the 28th 2022)
33. Flaxel CJ, Adelman RA, Bailey ST, Fawzi A, Lim JI, Vemulakonda GA, Ying GS. (2020) Diabetic Retinopathy Preferred Practice Pattern(R). Ophthalmology, 127: P66-P145.

34. Kras A, Celi LA, Miller JB. (2020) Accelerating ophthalmic artificial intelligence research: the role of an open access data repository. Curr Opin Ophthalmol, 31: 337-350.
35. OECD. (2018) Computed tomography (CT) exams.https://doi.org/10.1787/3c994537-en (last accessed on February the 28th 2022)
36. De Fauw J, Ledsam JR, Romera-Paredes B, Nikolov S, Tomasev N, Blackwell S, Askham H, Glorot X, O'Donoghue B, Visentin D, van den Driessche G, Lakshminarayanan B, Meyer C, Mackinder F, Bouton S, Ayoub K, Chopra R, King D, Karthikesalingam A, Hughes CO, Raine R, Hughes J, Sim DA, Egan C, Tufail A, Montgomery H, Hassabis D, Rees G, Back T, Khaw PT, Suleyman M, Cornebise J, Keane PA, Ronneberger O. (2018) Clinically applicable deep learning for diagnosis and referral in retinal disease. Nat Med, 24: 1342-1350.
37. (1991) Grading diabetic retinopathy from stereoscopic color fundus photographs--an extension of the modified Airlie House classification. ETDRS report number 10. Early Treatment Diabetic Retinopathy Study Research Group. Ophthalmology, 98: 786-806.
38. Nagi DK, Gosden C, Walton C, Winocour PH, Turner B, Williams R, James J, Holt RI. (2009) A national survey of the current state of screening services for diabetic retinopathy: ABCD-diabetes UK survey of specialist diabetes services 2006. Diabet Med, 26: 1301-1305.
39. Stefansson E. (2006) Prevention of diabetic blindness. Br J Ophthalmol, 90: 2-3.
40. Williams GA, Scott IU, Haller JA, Maguire AM, Marcus D, McDonald HR. (2004) Single-field fundus photography for diabetic retinopathy screening: a report by the American Academy of Ophthalmology. Ophthalmology, 111: 1055-1062.
41. Pandey R, Morgan MM, Murphy C, Kavanagh H, Acheson R, Cahill M, McGettrick P, O'Toole L, Hamroush F, Mooney T, Byrne H, Fitzpatrick P, Keegan DJ. (2022) Irish National Diabetic RetinaScreen Programme: report on five rounds of retinopathy screening and screen-positive referrals. (INDEAR study report no. 1). Br J Ophthalmol, 106: 409-414.

42. Munk MR, Somfai GM, de Smet MD, Donati G, Menke MN, Garweg JG, Ceklic L. (2022) The Role of Intravitreal Corticosteroids in the Treatment of DME: Predictive OCT Biomarkers. Int J Mol Sci, 23.
43. Delia Cabrera DeBuc (2011). A Review of Algorithms for Segmentation of Retinal Image Data Using Optical Coherence Tomography, Image Segmentation, Dr. Pei-Gee Ho (Ed.), ISBN: 978-953-307-228-9, InTech, Available from: http://www.intechopen.com/books/image-segmentation/a-review-of-algorithms-forsegmentation-of-retinal-image-data-using-optical-coherence-tomography (last accessed on August the 28th 2022) : 15-54
44. Knighton RW, Gregori G. (2012) The shape of the ganglion cell plus inner plexiform layers of the normal human macula. Invest Ophthalmol Vis Sci, 53: 7412-7420.
45. Schaudig UH, Glaefke C, Scholz F, Richard G. (2000) Optical coherence tomography for retinal thickness measurement in diabetic patients without clinically significant macular edema. Ophthalmic Surg Lasers, 31: 182-186.
46. Oshitari T, Hanawa K, Adachi-Usami E. (2009) Changes of macular and RNFL thicknesses measured by Stratus OCT in patients with early stage diabetes. Eye (Lond), 23: 884-889.
47. Bizheva K, Pflug R, Hermann B, Povazay B, Sattmann H, Qiu P, Anger E, Reitsamer H, Popov S, Taylor JR, Unterhuber A, Ahnelt P, Drexler W. (2006) Optophysiology: depth-resolved probing of retinal physiology with functional ultrahigh-resolution optical coherence tomography. Proc Natl Acad Sci U S A, 103: 5066-5071.
48. Tan O, Li G, Lu AT, Varma R, Huang D, Advanced Imaging for Glaucoma Study G. (2008) Mapping of macular substructures with optical coherence tomography for glaucoma diagnosis. Ophthalmology, 115: 949-956.
49. Alam M, Zhang Y, Lim JI, Chan RVP, Yang M, Yao X. (2020) Quantitative Optical Coherence Tomography Angiography Features for Objective Classification and Staging of Diabetic Retinopathy. Retina, 40: 322-332.
50. Gavrilova Y., https://serokell.io/blog/ai-ml-dl-difference (last accessed on August the 13th 2022)

51. DeBuc DC. (2020) Artificial intelligence in the ophthalmic landscape. Nepal J Ophthalmol, 12: 1-3.
52. Ting DSW, Pasquale LR, Peng L, Campbell JP, Lee AY, Raman R, Tan GSW, Schmetterer L, Keane PA, Wong TY. (2019) Artificial intelligence and deep learning in ophthalmology. Br J Ophthalmol, 103: 167-175.
53. Loo J, Clemons TE, Chew EY, Friedlander M, Jaffe GJ, Farsiu S. (2020) Beyond Performance Metrics: Automatic Deep Learning Retinal OCT Analysis Reproduces Clinical Trial Outcome. Ophthalmology, 127: 793-801.
54. Naz H, Ahuja S. (2020) Deep learning approach for diabetes prediction using PIMA Indian dataset. J Diabetes Metab Disord, 19: 391-403.
55. Zhang K, Liu X, Xu J, Yuan J, Cai W, Chen T, Wang K, Gao Y, Nie S, Xu X, Qin X, Su Y, Xu W, Olvera A, Xue K, Li Z, Zhang M, Zeng X, Zhang CL, Li O, Zhang EE, Zhu J, Xu Y, Kermany D, Zhou K, Pan Y, Li S, Lai IF, Chi Y, Wang C, Pei M, Zang G, Zhang Q, Lau J, Lam D, Zou X, Wumaier A, Wang J, Shen Y, Hou FF, Zhang P, Xu T, Zhou Y, Wang G. (2021) Deep-learning models for the detection and incidence prediction of chronic kidney disease and type 2 diabetes from retinal fundus images. Nat Biomed Eng, 5: 533-545.
56. Trucco E, Ruggeri A, Karnowski T, Giancardo L, Chaum E, Hubschman JP, Al-Diri B, Cheung CY, Wong D, Abramoff M, Lim G, Kumar D, Burlina P, Bressler NM, Jelinek HF, Meriaudeau F, Quellec G, Macgillivray T, Dhillon B. (2013) Validating retinal fundus image analysis algorithms: issues and a proposal. Invest Ophthalmol Vis Sci, 54: 3546-3559.
57. Li JO, Liu H, Ting DSJ, Jeon S, Chan RVP, Kim JE, Sim DA, Thomas PBM, Lin H, Chen Y, Sakomoto T, Loewenstein A, Lam DSC, Pasquale LR, Wong TY, Lam LA, Ting DSW. (2021) Digital technology, tele-medicine and artificial intelligence in ophthalmology: A global perspective. Prog Retin Eye Res, 82: 100900.
58. Khan SM, Liu X, Nath S, Korot E, Faes L, Wagner SK, Keane PA, Sebire NJ, Burton MJ, Denniston AK. (2021) A global review of publicly available datasets for ophthalmological imaging: barriers to access, usability, and generalisability. Lancet Digit Health, 3: e51-e66.

59. Panch T, Pollard TJ, Mattie H, Lindemer E, Keane PA, Celi LA. (2020) "Yes, but will it work for my patients?" Driving clinically relevant research with benchmark datasets. NPJ Digit Med, 3: 87.
60. Brady CJ, Villanti AC, Pearson JL, Kirchner TR, Gupta OP, Shah CP. (2014) Rapid grading of fundus photographs for diabetic retinopathy using crowdsourcing. J Med Internet Res, 16: e233.
61. Brady CJN, F.; Wolle, M.A.; Mkocha, H; West, S.K. (2021) Crowdsourcing Can Match Field Grading Validity for Follicular Trachoma. In: ARVO 2021 Vol. 62 p. 1788
62. Abramoff MD, Lavin PT, Birch M, Shah N, Folk JC. (2018) Pivotal trial of an autonomous AI-based diagnostic system for detection of diabetic retinopathy in primary care offices. NPJ Digit Med, 1: 39.
63. Ipp E, Liljenquist D, Bode B, Shah VN, Silverstein S, Regillo CD, Lim JI, Sadda S, Domalpally A, Gray G, Bhaskaranand M, Ramachandra C, Solanki K, EyeArt Study G. (2021) Pivotal Evaluation of an Artificial Intelligence System for Autonomous Detection of Referrable and Vision-Threatening Diabetic Retinopathy. JAMA Netw Open, 4: e2134254.
64. Johnson LE, Larsen M, Perez MT. (2013) Retinal adaptation to changing glycemic levels in a rat model of type 2 diabetes. PLoS One, 8: e55456.
65. Enzsoly A, Szabo A, Szabo K, Szel A, Nemeth J, Lukats A. (2015) Novel features of neurodegeneration in the inner retina of early diabetic rats. Histol Histopathol, 30: 971-985.
66. Szabo K, Enzsoly A, Dekany B, Szabo A, Hajdu RI, Radovits T, Matyas C, Olah A, Laurik LK, Somfai GM, Merkely B, Szel A, Lukats A. (2017) Histological Evaluation of Diabetic Neurodegeneration in the Retina of Zucker Diabetic Fatty (ZDF) Rats. Sci Rep, 7: 8891.
67. Somfai GM, Tatrai E, Laurik L, Varga B, Olvedy V, Jiang H, Wang J, Smiddy WE, Somogyi A, DeBuc DC. (2014) Automated classifiers for early detection and diagnosis of retinopathy in diabetic eyes. BMC Bioinformatics, 15: 106.
68. Verma A, Rani PK, Raman R, Pal SS, Laxmi G, Gupta M, Sahu C, Vaitheeswaran K, Sharma T. (2009) Is neuronal dysfunction an early sign of diabetic retinopathy? Microperimetry and spectral domain optical coherence

tomography (SD-OCT) study in individuals with diabetes, but no diabetic retinopathy. Eye (Lond), 23: 1824-1830.

69. Cabrera Fernandez D, Salinas HM, Puliafito CA. (2005) Automated detection of retinal layer structures on optical coherence tomography images. Opt Express, 13: 10200-10216.
70. Varga BE, Gao W, Laurik KL, Tatrai E, Simo M, Somfai GM, Cabrera DeBuc D. (2015) Investigating Tissue Optical Properties and Texture Descriptors of the Retina in Patients with Multiple Sclerosis. PLoS One, 10: e0143711.
71. Hageman GS, Marmor MF, Yao XY, Johnson LV. (1995) The interphotoreceptor matrix mediates primate retinal adhesion. Arch Ophthalmol, 113: 655-660.
72. Costa RA, Skaf M, Melo LA, Jr., Calucci D, Cardillo JA, Castro JC, Huang D, Wojtkowski M. (2006) Retinal assessment using optical coherence tomography. Prog Retin Eye Res, 25: 325-353.
73. Cabrera DeBuc D, Somfai GM. (2010) Early detection of retinal thickness changes in diabetes using Optical Coherence Tomography. Med Sci Monit, 16: MT15-21.
74. Gao WT, E.; Somfai, G. M.; Cabrera, D. C. (2011) Assessing the performance of optical properties determination of intraretinal layers in healthy normal and type 1 diabetic eyes using optical coherence tomography Vol. 52 pp. 4-22
75. Matyas C, Nemeth BT, Olah A, Torok M, Ruppert M, Kellermayer D, Barta BA, Szabo G, Kokeny G, Horvath EM, Bodi B, Papp Z, Merkely B, Radovits T. (2017) Prevention of the development of heart failure with preserved ejection fraction by the phosphodiesterase-5A inhibitor vardenafil in rats with type 2 diabetes. Eur J Heart Fail, 19: 326-336.
76. Hajdu RI, Laurik LK, Szabo K, Dekany B, Almasi Z, Enzsoly A, Szabo A, Radovits T, Matyas C, Olah A, Szel A, Somfai GM, David C, Lukats A. (2019) Detailed Evaluation of Possible Ganglion Cell Loss in the Retina of Zucker Diabetic Fatty (ZDF) Rats. Sci Rep, 9: 10463.
77. Nadal-Nicolas FM, Jimenez-Lopez M, Sobrado-Calvo P, Nieto-Lopez L, Canovas-Martinez I, Salinas-Navarro M, Vidal-Sanz M, Agudo M. (2009) Brn3a as a marker of retinal ganglion cells: qualitative and quantitative time

course studies in naive and optic nerve-injured retinas. Invest Ophthalmol Vis Sci, 50: 3860-3868.

78. Charalambous P, Wang X, Thanos S, Schober A, Unsicker K. (2013) Regulation and effects of GDF-15 in the retina following optic nerve crush. Cell Tissue Res, 353: 1-8.
79. Kwong JM, Caprioli J, Piri N. (2010) RNA binding protein with multiple splicing: a new marker for retinal ganglion cells. Invest Ophthalmol Vis Sci, 51: 1052-1058.
80. Xiang M, Zhou L, Macke JP, Yoshioka T, Hendry SH, Eddy RL, Shows TB, Nathans J. (1995) The Brn-3 family of POU-domain factors: primary structure, binding specificity, and expression in subsets of retinal ganglion cells and somatosensory neurons. J Neurosci, 15: 4762-4785.
81. Belforte N, Sande PH, de Zavalia N, Dorfman D, Rosenstein RE. (2012) Therapeutic benefit of radial optic neurotomy in a rat model of glaucoma. PLoS One, 7: e34574.
82. Szabo K, Szabo A, Enzsoly A, Szel A, Lukats A. (2014) Immunocytochemical analysis of misplaced rhodopsin-positive cells in the developing rodent retina. Cell Tissue Res, 356: 49-63.
83. Li TG, Y.; Wang, K.; Guo, S.; Liu, H.; Kanga, H. (2019) Diagnostic assessment of deep learning algorithms for diabetic retinopathy screening. Information Sciences, 501: 511-522.
84. Cuadros J, Bresnick G. (2009) EyePACS: an adaptable telemedicine system for diabetic retinopathy screening. J Diabetes Sci Technol, 3: 509-516.
85. Fleming AD, Philip S, Goatman KA, Olson JA, Sharp PF. (2006) Automated assessment of diabetic retinal image quality based on clarity and field definition. Invest Ophthalmol Vis Sci, 47: 1120-1125.
86. Gulshan V, Peng L, Coram M, Stumpe MC, Wu D, Narayanaswamy A, Venugopalan S, Widner K, Madams T, Cuadros J, Kim R, Raman R, Nelson PC, Mega JL, Webster DR. (2016) Development and Validation of a Deep Learning Algorithm for Detection of Diabetic Retinopathy in Retinal Fundus Photographs. JAMA, 316: 2402-2410.

87. Zapata MA, Royo-Fibla D, Font O, Vela JI, Marcantonio I, Moya-Sanchez EU, Sanchez-Perez A, Garcia-Gasulla D, Cortes U, Ayguade E, Labarta J. (2020) Artificial Intelligence to Identify Retinal Fundus Images, Quality Validation, Laterality Evaluation, Macular Degeneration, and Suspected Glaucoma. Clin Ophthalmol, 14: 419-429.
88. Laurik-Feuerstein KL, Sapahia R, Cabrera DeBuc D, Somfai GM. (2022) The assessment of fundus image quality labeling reliability among graders with different backgrounds. PLoS One, 17: e0271156.
89. Nadal-Nicolas FM, Jimenez-Lopez M, Salinas-Navarro M, Sobrado-Calvo P, Alburquerque-Bejar JJ, Vidal-Sanz M, Agudo-Barriuso M. (2012) Whole number, distribution and co-expression of brn3 transcription factors in retinal ganglion cells of adult albino and pigmented rats. PLoS One, 7: e49830.
90. Ackland P, Resnikoff S, Bourne R. (2017) World blindness and visual impairment: despite many successes, the problem is growing. Community Eye Health, 30: 71-73.
91. Flaxman SR, Bourne RRA, Resnikoff S, Ackland P, Braithwaite T, Cicinelli MV, Das A, Jonas JB, Keeffe J, Kempen JH, Leasher J, Limburg H, Naidoo K, Pesudovs K, Silvester A, Stevens GA, Tahhan N, Wong TY, Taylor HR, Vision Loss Expert Group of the Global Burden of Disease S. (2017) Global causes of blindness and distance vision impairment 1990-2020: a systematic review and meta-analysis. Lancet Glob Health, 5: e1221-e1234.
92. Hammes HP. (2018) Diabetic retinopathy: hyperglycaemia, oxidative stress and beyond. Diabetologia, 61: 29-38.
93. Lechner J, O'Leary OE, Stitt AW. (2017) The pathology associated with diabetic retinopathy. Vision Res, 139: 7-14.
94. Chihara E, Matsuoka T, Ogura Y, Matsumura M. (1993) Retinal nerve fiber layer defect as an early manifestation of diabetic retinopathy. Ophthalmology, 100: 1147-1151.
95. Sokol S, Moskowitz A, Skarf B, Evans R, Molitch M, Senior B. (1985) Contrast sensitivity in diabetics with and without background retinopathy. Arch Ophthalmol, 103: 51-54.

96. Bearse MA, Jr., Han Y, Schneck ME, Barez S, Jacobsen C, Adams AJ. (2004) Local multifocal oscillatory potential abnormalities in diabetes and early diabetic retinopathy. Invest Ophthalmol Vis Sci, 45: 3259-3265.

97. van Dijk HW, Verbraak FD, Kok PH, Stehouwer M, Garvin MK, Sonka M, DeVries JH, Schlingemann RO, Abramoff MD. (2012) Early neurodegeneration in the retina of type 2 diabetic patients. Invest Ophthalmol Vis Sci, 53: 2715-2719.

98. van Dijk HW, Verbraak FD, Kok PH, Garvin MK, Sonka M, Lee K, Devries JH, Michels RP, van Velthoven ME, Schlingemann RO, Abramoff MD. (2010) Decreased retinal ganglion cell layer thickness in patients with type 1 diabetes. Invest Ophthalmol Vis Sci, 51: 3660-3665.

99. Rashmi MM, R.; Crosby-Nwaobi, R.; Abdelhay, A.; Sivaprasad, S.; Heng, S. (2012) Retinal neuronal changes in people with diabetes., p. 2852

100. Abramoff MD, Kwon YH, Ts'o D, Soliz P, Zimmerman B, Pokorny J, Kardon R. (2006) Visual stimulus-induced changes in human near-infrared fundus reflectance. Invest Ophthalmol Vis Sci, 47: 715-721.

101. Grieve K, Roorda A. (2008) Intrinsic signals from human cone photoreceptors. Invest Ophthalmol Vis Sci, 49: 713-719.

102. Schmidt-Erfurth U, Sadeghipour A, Gerendas BS, Waldstein SM, Bogunovic H. (2018) Artificial intelligence in retina. Prog Retin Eye Res, 67: 1-29.

103. Yanagihara RT, Lee CS, Ting DSW, Lee AY. (2020) Methodological Challenges of Deep Learning in Optical Coherence Tomography for Retinal Diseases: A Review. Transl Vis Sci Technol, 9: 11.

104. Barber AJ, Lieth E, Khin SA, Antonetti DA, Buchanan AG, Gardner TW. (1998) Neural apoptosis in the retina during experimental and human diabetes. Early onset and effect of insulin. J Clin Invest, 102: 783-791.

105. Kern TS, Barber AJ. (2008) Retinal ganglion cells in diabetes. J Physiol, 586: 4401-4408.

106. McKenna M, Chen T, McAneney H, Vazquez Membrillo MA, Jin L, Xiao W, Peto T, He M, Hogg R, Congdon N. (2018) Accuracy of trained rural ophthalmologists versus non-medical image graders in the diagnosis of diabetic retinopathy in rural China. Br J Ophthalmol, 102: 1471-1476.

107. Islam FMA. (2017) Accuracy and reliability of retinal photo grading for diabetic retinopathy: Remote graders from a developing country and standard retinal photo grader in Australia. PLoS One, 12: e0179310.

108. Thapa R, Bajimaya S, Bouman R, Paudyal G, Khanal S, Tan S, Thapa SS, van Rens G. (2016) Intra- and inter-rater agreement between an ophthalmologist and mid-level ophthalmic personnel to diagnose retinal diseases based on fundus photographs at a primary eye center in Nepal: the Bhaktapur Retina Study. BMC Ophthalmol, 16: 112.

9. BIBLIOGRAPHY OF PUBLICATIONS

Publications related to the thesis:

Laurik-Feuerstein KL1, Sapahia R1, DeBuc DC, Somfai GM. The assessment of fundus image quality labeling reliability among graders with different backgrounds. PLOS ONE 17: 7 Paper: 0271156, 11 p. (2022)
1Megosztott első szerzők
IF: 3,752*

Hajdú Rozina I, Laurik LK, Szabó K, Dékány B, Almási Z, Énzsöly A, Szabó A, Radovits T, Mátyás C, Oláh A, Szél Á, Somfai GM, Dávid C, Lukáts Á. Detailed Evaluation of Possible Ganglion Cell Loss in the Retina of Zucker Diabetic Fatty (ZDF) Rats. SCIENTIFIC REPORTS 9: 1 Paper: 10463, 16 p. (2019)
IF: 3,998

Somfai GM, Tatrai E, Laurik L, Varga B, Olvedy V, Jiang H, Wang J, Smiddy WE, Somogyi A, Debuc DC. Automated classifiers for early detection and diagnosis of retinopathy in diabetic eyes. BMC BIOINFORMATICS 15 Paper: 106, 10 p. (2014)
IF: 2,576

* expected IF

Publications not related to the thesis:

Szentmary Nora, Fries Fabian Norbert, Daas Loay, Shi Lei, Laurik Kornelia Lenke, Langenbucher Achim, Seitz Berthold. Chamäleonartige Hornhautveränderungen: Akanthamöben-keratitis [Chameleon-Like CornealDisorders: Acanthamoeba Keratitis].KLINISCHE MONATSBLATTER FUR AUGENHEILKUNDE 237: 6 pp. 754-760.(2020)
IF: 0,700

Laurik Kornélia Lenke, Milioti Georgia, Abdin Alaadin, Leonhard Marie, Tsintarakis Themistoklis, Seitz Berthold. Retinaler Venenverschluss – atypische Erstmanifestation

der okulären Toxoplasmose [Retinal Vein Occlusion–Atypical Primary Manifestationof Ocular Toxoplasmosis]. KLINISCHE MONATSBLATTER FUR AUGENHEILKUNDE 237: 8 pp. 976-979. (2020)
IF: 0,700

Laurik Kornélia Lenke, Szentmáry Nóra, Daas Loay, Langenbucher Achim, Seitz Berthold. Early Penetrating Keratoplasty À Chaud May Improve Outcome in Therapy-Resistant Acanthamoeba Keratitis ADVANCES IN THERAPY 36: 9 pp. 2528-2540. (2019)
IF: 3,871

Szentmáry N, Daas L, Shi L, Laurik KL, Lepper S, Milioti G, Seitz B. Acanthamoeba keratitis – Clinical signs, differential diagnosis and treatment. JOURNAL OF CURRENT OPHTHALMOLOGY 31: 1 pp. 16-23. (2019)

Szentmary N, Daas L, Shi L, Laurik KL, Seitz B. Akanthamobenkeratitis – klinische Zeichen, Diagnose, Therapie [Acanthamobenkeratitis – Clinical Signs, Diagnosis, Therapy]. KLINISCHE MONATSBLATTER FUR AUGENHEILKUNDE 235: 6 pp. 671-677. (2018)
IF: 0,792

Szabo K, Enzsoly A, Dekany B, Szabo A, Hajdu RI, Radovits T, Matyas C, Olah A, Laurik Kornelia Lenke, Somfai GM, Merkely B, Szel A, Lukats A. Histological Evaluation of Diabetic Neurodegeneration in the Retina of Zucker Diabetic Fatty (ZDF) Rats. SCIENTIFIC REPORTS 7: 1 Paper: 8891, 17 p. (2017)
IF: 4,122

Szentmary N, Modis L, Imre L, Fust A, Daas L, Laurik L, Seitz B, Nagy ZZ. Fertőzéses keratitisek diagnosztikája és kezelése [Diagnostics and treatment of infectious keratitis]. ORVOSI HETILAP 158: 31 pp. 1203-1212. (2017)
IF: 0,322

Varga BE, Gao W, Laurik KL, Tatrai E, Simo M, Somfai GM, Cabrera DeBuc D. Investigating Tissue Optical Properties and Texture Descriptors of the Retina in Patients with Multiple Sclerosis. PLOS ONE 10: 11 Paper: e0143711, 20 p. (2015)
IF: 3,057

Somfai GM, Tatrai E, Laurik L, Varga BE, Olvedy V, Smiddy WE, Tchitnga R, Somogyi A, DeBuc DC. Fractal-based analysis of optical coherence tomography data to quantify retinal tissue damage. BMC BIOINFORMATICS 15: 1 Paper: 295, 10 p. (2014)
IF: 2,576

Delia DeBuc, Tatrai Erika, Laurik Lenke, Varga Boglarka Eniko, Veronika Olvedy, Somogyi Aniko, William E Smiddy, Somfai Gabor Mark. Identifying Local Structural and Optical Derangement in the Neural Retina of Individuals with Type 1 Diabetes. JOURNAL OF CLINICAL AND EXPERIMENTAL OPHTHALMOLOGY 4: 4 Paper: 1000289, 9 p. (2013)

∑IF: 26,466

DOI:10.14753/SE.2023.2807

10. ACKNOWLEDGEMENTS

Throughout my scientific work, I have received essential and selfless support and assistance from a number of individuals.

First, I would like to thank my supervisor Gábor Márk Somfai PhD and my external advisor Delia Cabrera DeBuc PhD for their support and guidance during the several years of our work together. I would like to thank both of them for their patience and their always wise council and empathic advice to inspire and engage my interest for our research as a medical student and to give me several opportunities to follow through until completing this dissertation. I did so, while becoming a mother and a specialist for ophthalmology. In a lot of ways, thank to you.

I would like to thank my fellow researchers and colleagues who have worked together on research, data collection, data analysis, statistical evaluation, and preparation of scientific work for publication, especially Rozina Ida Hajdú, Rishav Sapahia, Boglárka Enikő Varga PhD, Anna Bakos-Kiss PhD, Irén Szalai, Erika Tátrai PhD, Ákos Lukáts PhD, Klaudia Szabó PhD, Csaba Dávid Phd és Arnold Szabó for their help in designing and carrying out the methodological background of the research and Prof. Zoltán Zsolt Nagy DSc an Prof. Ágoston Szél DSc for providing the opportunity to carry out the research at their Institute.
I would also like to thank the Éva Kovácsné Dobozi and Nikolett Májer Dóczi for their valuable work and help through the histological experiments, as well as László Laurik, Viviane Guignard, Martin Lörtscher, Irén Szalai, Marco Feuerstein and László Miklós Laurik for their time and effort performing the grading task of the image labelling study.

Special thanks to Marianna Kondorosiné Török PhD and all members of the Workgroup for Science Management, Doctoral School, for their support in writing my dissertation and completing it as soon as possible

And finally, I would like to thank my family and friends for their understanding and support during the whole process.